Geophysical Journal International

Geophys. J. Int. (2012) **189,** 1253–1276 doi: 10.1111/j.1365-246X.2012.05427.x

Lithosphere–mantle coupling and the dynamics of the Eurasian Plate

Karin N. Warners-Ruckstuhl, Rob Govers and Rinus Wortel

Department of Earth sciences, Utrecht University, P.O. Box 80.021, 3508 *TA Utrecht, the Netherlands. E-mail: ruckstuh@geo.uu.nl*

Accepted 2012 February 20. Received 2012 February 12; in original form 2011 August 2

SUMMARY

Mechanical equilibrium of tectonic plates implies that lithospheric edge and body forces are balanced by forces arising from interaction with the underlying mantle. We use this quantitative physical relation to integrate existing modelling approaches of lithosphere dynamics and mantle flow into a new combined approach applied to the Eurasian Plate. By combining a thorough analysis of lithospheric forces with the requirement of torque balance we constrain the orientation of the torque on Eurasia arising from mantle tractions. We use this constraint to evaluate convective mantle flow models driven by tomographic or subduction history model anomalies and observed plate motion. Mantle forcing is considered through both shear at the bottom of the plate and induced dynamic topography. We find that instantaneous semi-analytic flow models without lateral viscosity variations generate tractions that meet the constraint from Eurasian lithosphere dynamics, but only for specific ranges of mantle flow parameters. Of the explored set of mantle anomaly models, only mantle flow models based on *S*-wave tomography anomalies can balance Eurasia for realistic viscosity profiles and velocity–density scaling. Choices in mantle density forcing and viscosity are crucial in that they govern the relative magnitude of tractions due to convective mantle flow ('active tractions') and resistive tractions due to plate motion ('passive tractions'). We find mechanical balance is only achieved for similar torque magnitudes of active and passive shear. The two shear contributions do however in no case balance each other and a considerable, dominant, net torque from edge forces is required to balance total mantle tractions and lithospheric body forces (LBFs). Our analysis provides a range of mechanically consistent total force sets acting on the Eurasian Plate. Using this result we find that mantle buoyancy forces and LBFs acting on Eurasia itself are important driving forces but do not drive Eurasia in the observed direction. Continental collision at Eurasia's southern boundary significantly deviates Eurasia northwards. Our combined torque balance approach, in which mantle tractions from convective mantle flow modelling are combined with explicitly applied edge forces, thus emphasizes the role of plate interactions to the dynamics of tectonic plates.

Key words: Plate motions; Dynamics of lithosphere and mantle; Neotectonics; Mechanics, theory, and modelling; Asia; Europe.

1 INTRODUCTION

The nature of mechanical coupling between the lithosphere and underlying mantle has been extensively debated since the advent of plate tectonics but is still poorly understood. Intrinsically linked to understanding lithosphere–mantle coupling is the question of which forces are the motor behind plate motion. Early studies on lithospheric driving forces, modelling coupling with the underlying mantle as passive drag against plate motion, identified slab pull and ridge push as the main plate driving forces (Forsyth & Uyeda 1975; Harper 1975; Richardson *et al.* 1979). More recently, mantle flow studies have demonstrated the importance of active mantle flow induced by density anomalies throughout the mantle in driving tectonic plates (Ricard & Vigny 1989; Lithgow-Bertelloni & Richards 1998; Becker & O'Connell 2001). How actual lithosphere–mantle interaction results from the above two contributions depends on mantle parameters like viscosity distribution and density anomalies driving the flow (Conrad & Lithgow-Bertelloni, 2002 2004; Becker 2006), which remain the subject of ongoing investigation Steinberger & Calderwood (2006); Simmons *et al.* (2009) [review article: Becker & Faccenna (2009)].

In this study, we aim to evaluate lithosphere–mantle coupling for the Eurasian Plate by combining lithospheric and mantle dynamics. Our analysis is based on mechanical equilibrium of tectonic plates which implies that, through torque balance, lithospheric edge and body forces must be counterbalanced by external forces arising from interaction with the underlying mantle (Forsyth & Uyeda 1975; Chapple & Tullis 1977). We build upon results presented by Warners-Ruckstuhl *et al.* (2010) (hereafter WR10), who analysed the lithospheric forces on the Eurasian Plate to constrain the

orientation of the torque resulting from mantle tractions at the base of the plate. This lithosphere-dynamic constraint on mantle tractions offers a simple test for models describing mantle flow. Interestingly, WR10 found that mantle tractions based on the classical approximation of uniform shear (anti)-parallel to absolute plate motion do not meet this constraint for Eurasia. Here, we evaluate whether tractions from convective global mantle flow models do mechanically balance Eurasia.

The constraint of torque balance can be seen as the basis in a hierarchy of constraints that should be met by models describing total sets of tectonic forces. Only models fulfilling torque balance can meaningfully be evaluated further based on observational constraints. Observed plate motions form a natural second step in constraining tectonic forces because they are sensitive to the integral of forces. Quantities that are sensitive to the exact distribution of the force field (e.g. stresses) form a third level of constraints. In this study, we focus on integrated quantities. In a follow-up study, we will proceed to evaluate successful models based on the observed stress field (Warners-Ruckstuhl *et al.*, in preparation).

We model the present mantle flow field by instantaneous flow in a viscous mantle driven by density anomalies based on various tomographic or geodynamic subduction-history models (Hager *et al.* 1985). Studies following this approach have shown successful results in several global mantle convection applications like reconstructing plate velocities (Lithgow-Bertelloni & Richards 1998; Becker & O'Connell 2001; Zhong 2001), lithospheric stresses (Steinberger *et al.* 2001; Lithgow-Bertelloni & Guynn 2004; Naliboff *et al.* 2009; Forte *et al.* 2010) and strain rate (Ghosh *et al.* 2008). To obtain realistic tractions at the base of Eurasia, we impose observed plate velocities as boundary conditions in the mantle flow field. Resulting tractions at the base of the lithosphere are the sum of two contributions (Ricard & Vigny 1989; Lithgow-Bertelloni & Silver 1998; Steinberger *et al.* 2001): (1) convective tractions generated by buoyancy forces inside the mantle (hereafter referred to as 'active tractions') and (2) resistance due to motion of the plates ('passive tractions'). The relative magnitude of both contributions indicates whether lithosphere–mantle coupling is dominated by drive from the mantle or from the plates and thus forms a good indication for the nature of the coupling. Because the ratio of active and passive tractions varies significantly depending on the assumed mantle buoyancy forcing and viscosity field it is not well constrained by mantle modelling alone. Here, we infer this ratio by making use of the external constraint of torque balance on the Eurasian Plate.

Torque balance has extensively been used to constrain tectonic forces previously. Studies doing so have generally focused either on the lithosphere, oversimplifying interaction with the underlying mantle (Forsyth & Uyeda 1975; Chapple & Tullis 1977; Wortel *et al.* 1991; Meijer & Wortel 1992; Govers & Meijer 2001; Liu & Bird 2002; Copley *et al.* 2010), or on the convecting mantle, neglecting edge forces due to plate interaction or implementing them through simplified rheological properties of plate boundaries (Ricard & Vigny 1989; Lithgow-Bertelloni & Richards 1998; Zhong 2001; Steinberger *et al.* 2001; Lithgow-Bertelloni & Guynn 2004; Ghosh *et al.* 2008). Both approaches yield a different application of the torque balance constraint. In the convecting mantle approach, in which plate velocities are solved for, torque balance is imposed on each plate taking into account passive tractions, active tractions and (in most cases) lithospheric body forces (LBFs). Edge forces result self-consistently from plate motion driven by gravitational forces, but are unlikely to be represented because they are governed by the ill-constrained imposed rheology of plate boundaries (Karpychev & Fleitout 1996; Čadek & Fleitout 1999). Because they are not considered in the torque balance calculations, a zero net torque due to edge forces is implicitly assumed on each plate (Steinberger *et al.* 2001). This restriction has no physical grounds. In the lithosphere-based approach, both edge forces and basal (mantle) tractions are parametrized based on observed plate motion. This introduces forcing which is not directly gravitational and requires that directions of boundary conditions be specified explicitly. Magnitudes of the parametrized forces are solved for such that torque balance occurs between mantle tractions, LBFs and edge forces. Typically, net edge force torques are considerable.

In recent years, a few global scale studies have merged both approaches and emphasized the need to simultaneously address the lithospheric and mantle system. Becker & O'Connell (2001) introduced parametrized edge forces (including slab pull) in a convecting mantle approach, but found that they could not significantly improve modelled plate motions due to their strong (anti-) correlation on the global scale. Conrad & Lithgow-Bertelloni (2002) concluded that adding a direct mechanical pull due to slabs in a mantle flow study considerably improves the match to observed plate motion. Bird *et al.* (2008) solved for basal shear stresses generating observed plate velocities in a lithospheric model in which edge forces arise self-consistently and are governed by friction coefficients on plate boundaries. They found that torques due to basal tractions, LBFs and edge forces are of comparable magnitude on most plates. Iaffaldano & Bunge (2009) coupled a geodynamic convection model to the lithospheric model of Bird *et al.* (2008) and showed that edge forces can be of significant magnitude relative to driving mantle buoyancy forces and can considerably affect plate motion.

In this study, we interface lithospheric and mantle modelling on a single-plate scale. We opt for a torque balance approach in which edge forces are modelled explicitly (and therefore may yield a non-zero net torque), and mantle tractions arise from mantle flow modelling. The plate-scale approach allows us to solve for the forces transmitted from adjacent plates without the need to make assumptions regarding the ill-constrained rheology of plate boundaries. It also allows for a more detailed resolution of edge forces than has been possible using a global-scale approach (Becker & O'Connell 2001). In our new single-plate approach, the interaction of the plate with the underlying mantle is exclusively represented by tractions from mantle flow models that contain active and passive tractions. The variability of these tractions is controlled by the uncertainty range of mantle flow parameters. A previous lithospheric-based single-plate model that incorporated active mantle tractions in a study of the North-American Plate (Humphreys & Coblentz 2007) concluded that mantle flow modelling results needed to be downscaled and complemented with a uniform shear to balance the plate and fit the observed stress field. In this study, we find that results from mantle flow modelling and lithospheric dynamics can be reconciled without the need to scale or add tractions.

We focus on the Eurasian Plate. Although for most tectonic plates on the Earth, the lithosphere-based torque balance method has produced force sets that were quite successful in reproducing the large-scale stress field, this is not the case for Eurasia (Goes *et al.* 2000). Convective mantle-based studies reproducing plate velocities or the first-order stress field on a global scale, did generally not produce particularly good results for the Eurasian part of their model (Steinberger *et al.* 2001; Lithgow-Bertelloni & Guynn 2004; Ghosh *et al.* 2008). The difficulty of capturing the forces controlling Eurasia seems to indicate that its dynamics cannot be approximated by concentrating on either the mantle or the lithosphere, but is governed by a combination of the two. This makes Eurasia an ideal plate to study

lithosphere–mantle coupling and the related issue of plate driving forces.

The novelty of what we present does not lie in the individual assessment of the forces, for which we use existing modelling approaches, but in the way we merge these results. By linking mantle flow tractions at the base of the lithosphere with a detailed analysis of lithospheric body and edge forces we require consistency between results from mantle- and lithosphere-dynamics modelling. The requirement of torque balance then creates the possibility to constrain remaining model uncertainties. It enables us to confine the nature of lithosphere–mantle coupling by solving for the ratio of active versus passive tractions required to balance the lithospheric forces on the Eurasian Plate. Subsequently, we use this result to analyse plate driving forces. Our analysis provides a range of mechanically consistent force sets acting on the Eurasian Plate in which mantle tractions, LBFs as well as edge forces play an important role. We evaluate the relative contributions of the three types of forces to the dynamics of Eurasia. Finally, by evaluating the force sets in the light of observed motion of Eurasia we identify which role the different tectonic forces play in driving Eurasia.

2 LITHOSPHERE-DYNAMICS CONSTRAINT ON MANTLE FLOW

2.1 Torque balance

Three types of forces act on tectonic plates: (1) edge forces due to interaction of a plate with neighbouring plates, (2) LBFs resulting from horizontal pressure gradients inside the lithosphere, caused by lateral variations in topography and density structure inside the lithosphere and (3) tractions at the bottom of the plate due to interaction with the underlying mantle. Mechanical equilibrium of tectonic plates implies that the sum of all torques on a plate vanishes (Forsyth & Uyeda 1975; Chapple & Tullis 1977). For a force distribution including N_{E} edge force types ${}_i\overline{F}_{\mathrm{E}}$ (with $i = 1, ..N_{\mathrm{E}}$), N_{B} LBF types ${}_i\overline{F}_{\mathrm{B}}$ and mantle tractions $\overline{F}_{\mathrm{M}}$:

$$\sum_{i=1}^{N_{\mathrm{E}}} \int_S \overline{r} \times {}_i\overline{F}_{\mathrm{E}}\, \mathrm{d}S + \sum_{i=1}^{N_{\mathrm{B}}} \int_V \overline{r} \times {}_i\overline{F}_{\mathrm{B}} \mathrm{d}V + \int_A \overline{r} \times \overline{F}_{\mathrm{M}}\, \mathrm{d}A = \overline{0}, \quad (1)$$

where the integration is over the boundary area S, the bottom area A or the volume V of the plate, while $\overline{r}$ is the position vector from the centre of the Earth.

Mantle tractions on the base of the lithosphere have shear and normal components, which both affect torque balance. The shear component directly contributes to the torque through the third integral of (1). The normal component induces dynamic topography that influences the gravitational potential energy (GPE) of the lithosphere (Hager *et al.* 1985; Lithgow-Bertelloni & Silver 1998). Lateral variations in GPE of the lithosphere result from topography and density variations inside the lithosphere, and induce LBFs (Artyushkov 1973; Fleitout & Froidevaux 1982; Molnar & Lyon-Cean 1988). Forces arising from the normal component of mantle tractions are therefore coupled to forces caused by the density structure of the lithosphere and enter eq. (1) via the second integral.

Edge forces result from mechanical interaction with neighbouring plates. We model their directions explicitly, so that they are independent of modelled mantle tractions. WR10 analysed edge forces on the Eurasian Plate and confined the direction of the total edge force torque (first term of eq. 1) on Eurasia. This result is based on the direction of forcing, inferred from the nature and geometry of the plate boundaries, and is independent of the poorly known magnitude of the edge forces. The orientation of the total edge force torque constrains the sum of the remaining, mantle-flow-dependent terms of (1), and forms the basis for our evaluation of mantle tractions. Below, we therefore present a summary of the analysis of edge forces previously outlined by WR10.

Pull due to downgoing slabs has been treated in different ways in the past. Essentially an LBF, in mantle flow models slabs are part of mantle buoyancies driving the flow and affect both downgoing and overriding plate through induced viscous flow. This treatment, however, does not directly incorporate the mechanical pull exerted by the slab on the surface part of the downgoing plate (Becker & O'Connell 2001; Conrad & Lithgow-Bertelloni 2002). In lithospheric torque balance models, slab pull has been incorporated as a quantified edge force. The only slab attached to the Eurasian Plate is the narrow section showing slab reversal in Taiwan and we choose to approximate its effect by incorporating it as part of the locally acting edge force.

2.2 Edge force torque

Following Forsyth & Uyeda (1975), edge forces are subdivided into categories based on tectonic setting (Fig. 1). Each edge force ${}_i\overline{F}_{\mathrm{E}}$ is parametrized as a constant magnitude per unit length of boundary ${}_iF_{\mathrm{E}}$ that represents the average contribution of processes beyond the boundary domain, and a unit vector $\overline{e}_i$ representing the relative motion direction. The torque contribution ${}_i\overline{T}_{\mathrm{E}}$ by edge force ${}_i\overline{F}_{\mathrm{E}}$ thus becomes

$${}_i\overline{T}_{\mathrm{E}} = \int_S \overline{r} \times {}_i\overline{F}_{\mathrm{E}}(\overline{r})\, \mathrm{d}S = {}_iF_{\mathrm{E}} \int_S \overline{r} \times \overline{e}_i(\overline{r})\, \mathrm{d}S = {}_iF_{\mathrm{E}}\, {}_i\overline{T}'_{\mathrm{E}}; \quad (2)$$

${}_i\overline{T}'_{\mathrm{E}}$ is an unscaled torque parallel to ${}_i\overline{T}_{\mathrm{E}}$.

Our model boundary for the Eurasian Plate follows the major plate boundaries (Bird 2003) where edge forces are most clearly defined (Fig. 1). We neglect features smaller than a few hundred kilometres and focus on the overall dynamics of Eurasia. By opting for a simple division of edge forces based on tectonic setting, we aim to represent the average force contribution of processes beyond our boundary domain. We distinguish five different edge force types (Fig. 1): (1) transform fault resistance on the ridge and transform boundary (red line), (2) continental collision force on the segments colliding with Africa, Arabia, India and Australia (black triangles), (3) forces at trench roll-back margins (purple triangles), (4) forces at non-roll-back margins (orange triangles) and (5) free boundary between continental North America and Eurasia, where the exact boundary location is unclear both in location and nature due to negligible relative velocities and the absence of seismicity or recent tectonic features (black line). Assuming normal and shear stresses are transmitted equally from one plate to another, resistive forces (transform fault resistance, continental collision and forces at non-roll-back subduction margins) are modelled antiparallel to the direction of motion relative to the adjacent plate [NUVEL-1a (DeMets *et al.* 1994)]. The force at subduction roll-back segments is expected to be dominated by suction of the retreating slab and is modelled outwards and perpendicular to the trench. Edge force magnitudes ${}_iF_{\mathrm{E}}$ are poorly known and not imposed *a priori*.

Torque orientations ${}_i\overline{T}'_{\mathrm{E}}$ for the various edge forces are displayed in Fig. 2. Geometrical properties of vector sums state that, for positive magnitudes ${}_iF_{\mathrm{E}}$, the orientation of the total edge force torque (first term in eq. 1) lies within the area enclosed by great-circles connecting the individual torques (WR10, red line in Fig. 2). The location inside this area depends on the relative magnitude of the different edge forces, and is further confined by physical

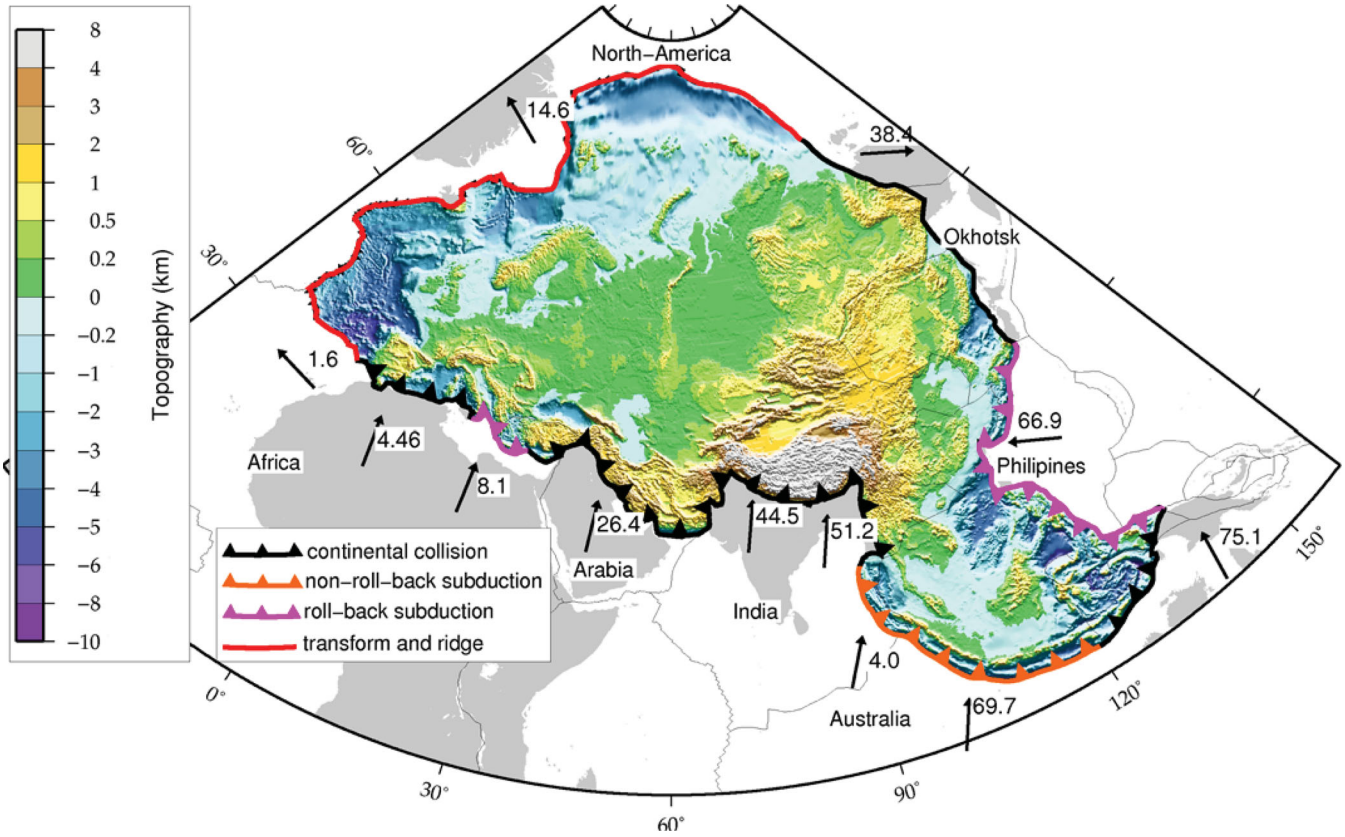

Figure 1. Topography and boundary types of Eurasian Plate model, after WR10. Arrows denote motion of adjacent plate with respect to Eurasia according to NUVEL-1a, rate of motion is indicated in mm yr^{-1}. Plate boundaries after Bird (2003). Our model Eurasian Plate follows major plate boundaries where edge forces are most easily defined.

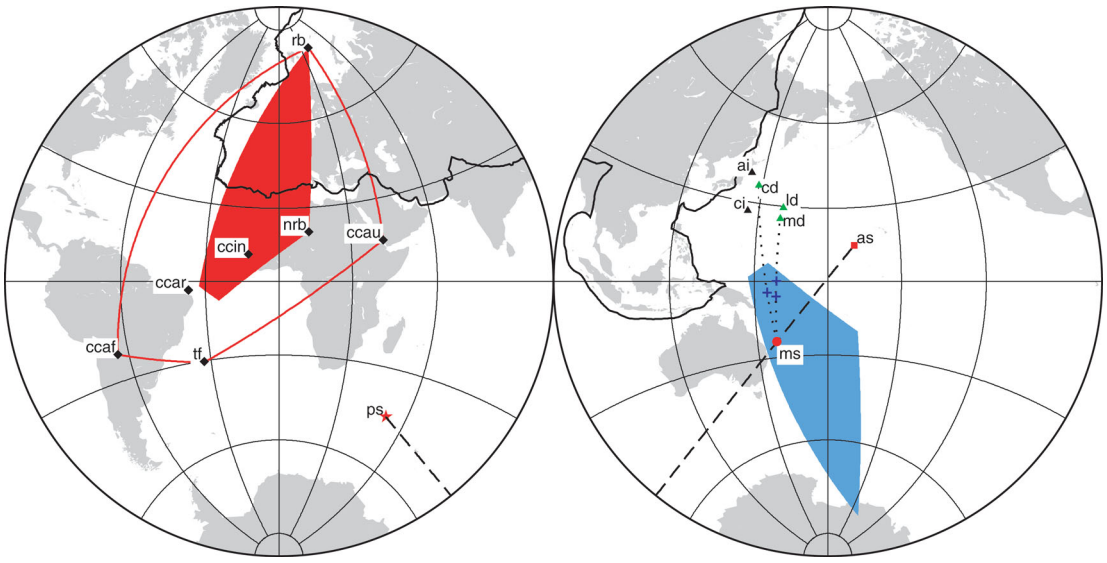

Figure 2. Representation of torque orientations of the various model forces for our example mantle flow model (based on tomographic model 'ngrand' (Grand 2002), v–ρ scaling factor 0.2 and viscosity profile (Mitrovica & Forte 2004). Positive ends of torque vectors are represented by their intersection with the globe in an upper hemisphere stereographic projection. Black diamonds: edge forces; Red: mantle shear; Black striped line is a great-circle segment connecting passive (star) and active (square) shear torques; it crosses the total shear torque (circle), which is the sum of the two. Triangles: LBFs; green: dynamic models, black: isostatically compensated models slightly modified after WR10 (ai: crustal Airy isostatic model, ci: isostatic Crust2.0 model). Blue crosses: sum of mantle shear and LBF torques, located on connecting great-circles segments (dotted lines). Red/blue zone represents physically acceptable range for the sum torque of all boundary forces and its antipodal area, respectively. Crosses in the blue zone represent force sets that enable torque balance of the Eurasian Plate. For abbreviations see Table A2.

restrictions therein. Based on the larger contact area per metre boundary we require: (1) continental collision boundaries to have a larger resistance per metre boundary than transform fault boundaries, and (2) continental collision resistance to be strongest on the contact segment with the Indian Plate. This restricts the orientation of the total edge force torque to the red area in Fig. 2. Inversely, it implies that all orientations inside the red area can result from realistic edge force distributions along the plate's boundary. Because the system is underdetermined (seven unknown edge force magnitudes, three degrees of freedom), each specific torque orientation inside the red zone can result from different combinations of individual edge forces. Our approach does not require that we solve for magnitudes of individual edge force types.

2.3 Implications for mantle flow

To mechanically balance Eurasia, LBFs and mantle tractions must counterbalance the total torque due to edge forces (eq. 1). The orientation of the edge force torque is confined to the red zone of Fig. 2 so that the orientation of the sum torque of mantle shear and LBFs should be located inside the antipodal blue zone. This constraint is relatively tight so that it allows us to evaluate mantle flow models for their ability to generate torques that can balance the Eurasian Plate.

3 MANTLE FLOW-DEPENDENT FORCING ON EURASIA

3.1 Mantle tractions

We calculate global mantle flow in a radially varying viscous mantle following the semi-analytical, propagator matrix approach in a spherical shell (Hager & O'Connell 1981). We use the graphical user interface SEATREE (Milner *et al.* 2009), which contains a modified implementation by Becker *et al.* (2006) based on Steinberger (2000). Mantle buoyancy fields are deduced from tomographic or subduction history models that have been expanded in spherical harmonics up to degree 31, corresponding to a wavelength of 1300 km. Since we are interested in mantle tractions actually felt by the Eurasian Plate, we impose observed plate motions as boundary conditions. Because our mantle flow models do not contain lateral viscosity variations (LVVs), no toroidal flow is excited and no net rotation of the lithosphere with respect to the mantle can be sustained (O'Connell *et al.* 1991). Any net rotation imposed on the lithosphere then simply results in a net rotation of the entire mantle with respect to the core, accommodated along the free-slip core–mantle interface. As a consequence, our modelled tractions at the base of the lithosphere reflect plate motions in a no-net-rotation (NNR) reference frame. In Section 8, we discuss the possible implications of net rotation of the lithosphere and show that it is not likely to significantly affect our conclusions.

We compute tractions at the base of a uniform 100-km-thick lithosphere for various mantle flow models, based on a variety of mantle buoyancy fields and (radial) viscosity profiles. The tractions from the mantle flow models are applied to a separate spherical thin shell lithospheric model for Eurasia (Fig. 1), on which we perform the torque calculations. The model domain is discretized using triangular elements of 50–100 km side length, which was tested to be dense enough that results are insensitive to further grid refinement.

To illustrate the methodology, we present resulting tractions for an example mantle flow model, which is representative for the family of models that we consider. In the subsequent torque analysis (Sections 4 and 5), we will present results for a broader range of models obtained with alternative choices regarding viscosity and mantle buoyancy, and discuss the consequences for torque balance of the Eurasian Plate.

Our example model's buoyancy field is derived from tomographic *S*-wave model 'ngrand' (Grand 2002). Seismic velocities are converted to densities assuming a constant velocity–density scaling (v–ρ scaling) of 0.2, which is around midway in the range suggested based on a thermal origin of wave speed anomalies (Steinberger & Calderwood 2006; Simmons *et al.* 2009). In the uppermost 250 km of the mantle beneath the continents, buoyancy variations due to temperature are probably largely cancelled by compositional variations (Goes & van der Lee 2002). Following previous studies (Lithgow-Bertelloni & Silver 1998; Becker & O'Connell 2001; Steinberger *et al.* 2001) we therefore remove the top 250 km of forcing. The flow field and corresponding tractions are calculated using the radial viscosity profile of Mitrovica & Forte (2004).

Resulting tractions at the base of the lithosphere are shown in Fig. 3. For linear flow laws as assumed in this study, total tractions can be viewed as the sum of two contributions (Ricard & Vigny 1989; Lithgow-Bertelloni & Silver 1998; Steinberger *et al.* 2001): (1) convective tractions due to flow driven by buoyancy forces inside the mantle under fixed plates (which we will refer to as 'active tractions'; Fig. 3a), and (2) tractions from flow driven by motions of plates over a other passive underlying mantle ('passive tractions'; Fig. 3b). Passive tractions on Eurasia are dominated by the resistance to absolute motion of the plate itself. Active tractions are typically of shorter wavelength. They are governed by upwellings and associated outward flow at mid-oceanic ridges (with strongest amplitude near the Iceland Hotspot) and downwellings and associated inward flow at subduction and collision zones. For the assumed mantle flow parameters, active tractions strongly dominate over passive ones, with magnitudes on average three times higher. Consequently, total mantle tractions (Fig. 3c) do not visibly show the imprint of absolute plate motion. However, we note that relative magnitudes of passive and active tractions strongly depend on mantle buoyancy magnitude and viscosity (see Sections 4.2 and 4.3).

3.2 LBFs including dynamic topography

LBFs arise from lateral variations in geopotential energy (GPE) of the lithosphere caused by topography and density structure variations (Artyushkov 1973; Fleitout & Froidevaux 1982; Molnar & Lyon-Cean 1988). They can be assessed when the density structure of the lithosphere is known. In the oceanic realm, cooling of the lithosphere causes the relatively well constrained ridge push (Lister 1975). In continental interiors and on passive margins, LBFs are more uncertain because the vertical density distribution of the lithosphere is less well constrained.

Normal mantle tractions cause uplift or subsidence of the entire lithosphere and thus affect LBFs. Focusing on long wavelength (neglecting flexure), we can assume pressure equilibrium at the base of the lithosphere between overburden pressure and dynamic pressure from the underlying mantle. Lateral variations in observed topography then arise from three contributions: (1) variations in crustal thickness and/or density, (2) variations in lithospheric mantle thickness and/or density and (3) variations in normal stress from the underlying mantle.

A number of studies have estimated topography resulting from the different contributions with the aim to reconcile results with observed topography, and showed that large wavelength deviations

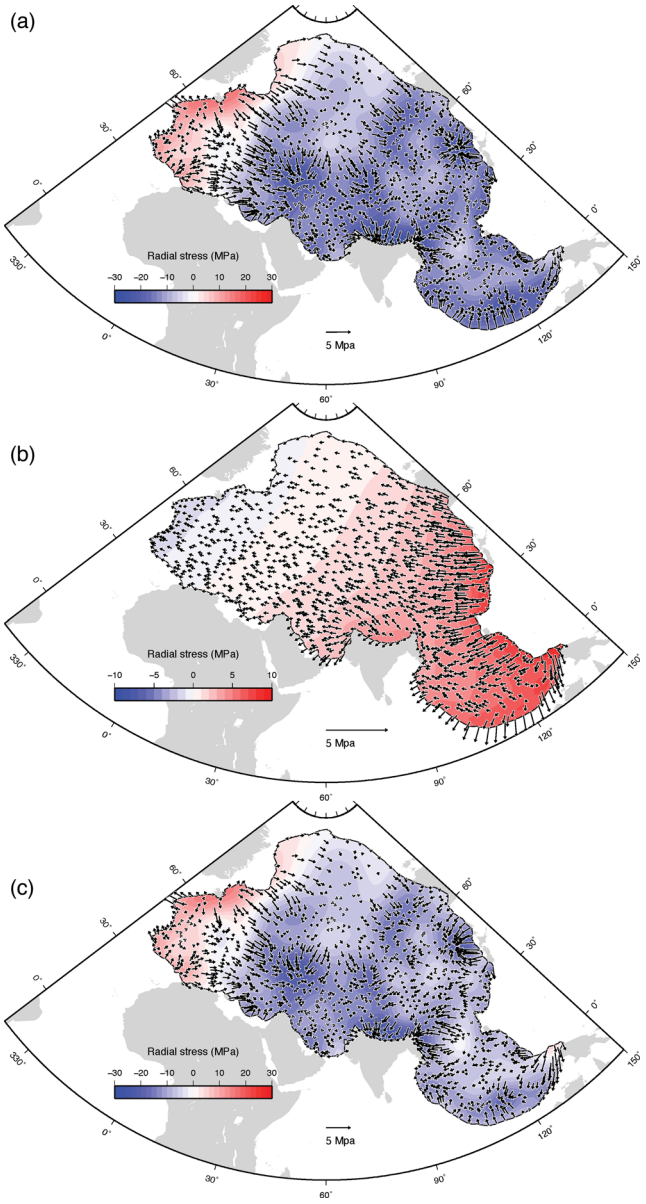

Figure 3. Mantle tractions at the base of the Eurasian Plate from global mantle flow model with density forcing deduced from tomographic model 'ngrand', viscosity profile of Mitrovica & Forte (2004) and imposed NNR plate velocities. Arrows represents shear stress, contour-colours radial stress, upward is positive. (a) Active tractions due to mantle buoyancies, (b) passive tractions due to motion of the plates over the mantle and (c) total tractions.

from isostatic equilibrium could indeed be matched to dynamic topography estimates from mantle flow models (Forte & Perry 2000; Conrad *et al.* 2004; Forte *et al.* 2010). However, uncertainties in observations of lithospheric structure and mantle flow modelling are such that topography estimates are consistent only to first order and generally do not add up to observed topography (Panasyuk & Hager 2000; Simmons *et al.* 2007). This hampers the combination of crustal and lithospheric structure observations into one lithospheric density model with mantle flow modelling results, while remaining consistent with observed topography. Studies combining the calculation of LBFs with mantle dynamics have adopted different approaches to circumvent this problem. While some have neglected the contribution from dynamic topography (Becker & O'Connell 2001; Flesch *et al.* 2007), most have modelled LBFs

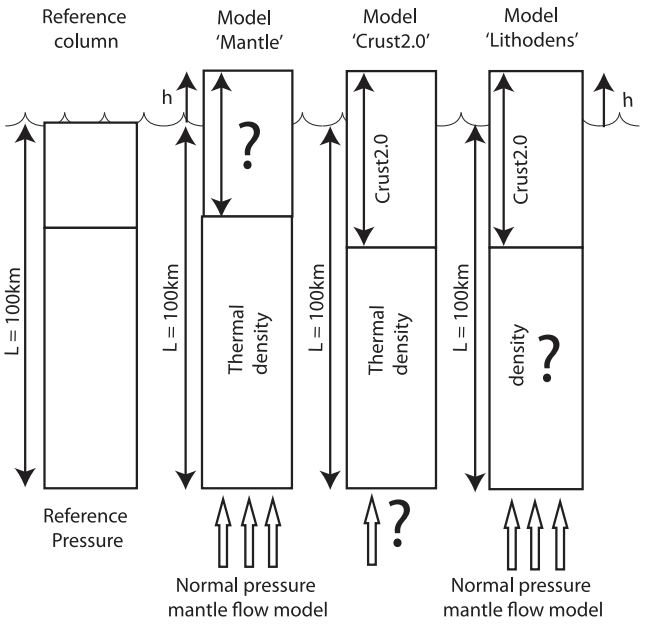

Figure 4. Topographic columns illustrating assumptions made in various LBF models. The question mark in each model represents the quantity that is calculated for the height of the column to match observed topography, being crustal thickness, normal mantle pressure and lithospheric density for models 'Mantle', 'Crust2.0' and 'Lithodens', respectively.

focusing on part of the available information. One possibility is to model LBFs using the observed crustal structure, and assume that deviations from isostatic equilibrium of the model are a result of the dynamic mantle (Lithgow-Bertelloni & Silver 1998; Ghosh *et al.*, 2008, 2009; Iaffaldano & Bunge 2009). Computed LBFs then include a dynamic component, but one that does not generally correlate with normal tractions from mantle flow modelling. Another possibility is to apply pressure variations from mantle flow modelling in combination with observed crustal thickness, and to adapt either crustal densities (Lithgow-Bertelloni & Silver 1998) or lithospheric mantle densities (Steinberger *et al.* 2001) to match the observed topography.

As we aim to evaluate mantle forcing on the lithosphere based on torque balance, it is important to assess the uncertainty in the torque generated by LBFs on the Eurasian Plate. We aim to cover the uncertainty range in lithospheric density structure by computing three different models. Each of the models assumes that the main uncertainty in defining the density structure of the lithosphere lies in a different unit, being the crust, the lithospheric mantle or dynamic mantle pressure at the base of the lithosphere. Fig. 4 illustrates the main elements of the three models. To remain consistent with the use of radially stratified mantle flow models, all three models assume a constant base of the lithosphere, taken to be 100 km. A short description of the models is given below, together with the presentation of the resulting GPE and force fields. We refer to the Appendix for computational details.

3.2.1 Model Mantle

Model 'Mantle' is based on dynamic topography deduced from normal mantle tractions at the base of the lithosphere from mantle flow modelling. On the continents and continental margins we assume that the part of the actual topography [ETOPO1 (Amante & Eakins 2009)] that is not dynamically supported is isostatically

compensated within the crust. We assume a constant crustal density and a temperature-dependent lithospheric density and compute crustal thicknesses that result in the observed topography. In the oceans, lithospheric structure and bathymetry is based on secular cooling and added to the dynamic topography component.

GPE and force distributions for model 'Mantle' depend on the normal component of mantle tractions and therefore vary as a function of mantle flow model. Results for our example mantle flow model are shown in Fig. 5(a). GPE varies both as a result of strong topography (Tibetan Plateau) and mantle tractions (high at Iceland and low in eastern Europe, see Fig. 3c). Variations due to both sources show approximately the same amplitude, indicating that radial pressure and crustal thickness variations have comparable influence on the force field.

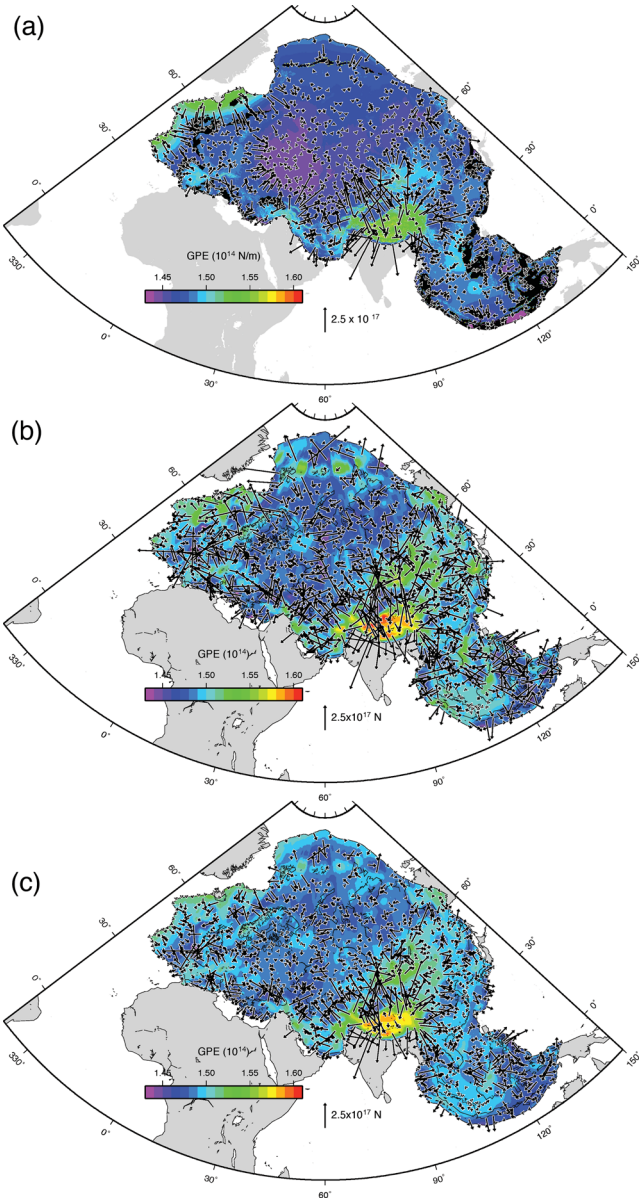

Figure 5. Force distribution (arrows) and GPE (contoured values) for the three LBF models including dynamic topography (see Fig. 4: (a) Model 'Mantle', (b) Model 'Crust2.0' and (c) Model 'Lithodens'. (Tomographic model 'ngrand', constant v–ρ-scaling 0.2, viscosity profile *MF*).

3.2.2 *Model Crust2.0*

Our second model is based on crustal thicknesses and densities of seismological model Crust2.0 (Bassin *et al.* 2000) and assumes that deviations from isostatic equilibrium are dynamically supported at the base of the lithosphere (Fig. 4). This model is comparable to models presented by Lithgow-Bertelloni & Silver (1998) and Ghosh *et al.* (2008, 2009). As in model 'Mantle', the lithospheric mantle density is temperature dependent (linear geotherm). To evaluate the compatibility of this model with mantle flow we compare the lithostatic pressures at the base of the lithosphere with normal stresses from mantle flow models (see the Appendix, Fig. A1). Although major features can be recognized in both models (e.g. the Iceland Hotspot and a large ring-like depression over central Eurasia), we find that differences are significant. Calculations based on an alternative crustal model Meier *et al.* (2007) lead to similar results. This confirms the need to investigate a range of models for the structure of the entire lithosphere, based on the different available data sets.

The resulting force distribution for model 'Crust2.0' (Fig. 5b) shows an outward pattern around the main topographical expression of Eurasia, the Tibetan Plateau, in agreement with observed gravitational collapse of elevated topography. However, whereas model 'Mantle' shows lower forcing outside the main mountain areas, the 'Crust2.0' model induces significant horizontal forces in regions lacking topography variations, caused by crustal structure variations that are not expressed in the topography. GPE variations occur on length scales, which are considerable smaller than in the mantle flow-based model 'Mantle', and the resulting force pattern is more chaotic.

3.2.3 *Model Lithodens*

In the third model, we combine crustal thickness and density from 'Crust2.0' with normal mantle tractions from mantle flow modelling and assume that uncertainty in the factors governing topography is entirely concentrated in the lithospheric mantle. We calculate averaged densities of the lithospheric mantle so that observed topography is matched (Fig. 4). This model is meant to capture the effects of variations in properties of the lithospheric mantle and is in essence comparable to the treatment of LBFs presented by Steinberger *et al.* (2001). Both lithospheric thickness and density are known to vary laterally but remain uncertain (Artemieva, 2003, 2006). Interpretation of seismic observations is ambiguous due to the combination of thermal and compositional effects (Forte & Perry 2000). Together, lithospheric thickness and density determine the total weight of the lithospheric mantle, which is the relevant factor towards topography. Again, to remain consistent with the use of radially stratified mantle flow models, we model variations in this weight by laterally varying lithospheric mantle density while keeping the depth of the lithosphere fixed to 100 km. This simplified weight distribution will affect resulting LBFs, and should be seen as a first-order approximation towards a more realistic model accounting for variable lithospheric thicknesses. Calculated densities range from 3050 to over 3500 kg m^{-3} (Fig. A2) exceeding, as expected, the realistic range in parts of the domain. Because they give an indication of the mass of the lithospheric mantle high densities can also indicate a thick lithospheric mantle. Qualitative comparison of calculated densities with lithospheric thicknesses presented by Artemieva (2006) shows that 'heavy' lithospheric mantle in Siberia and Scandinavia does correspond with regions of thick lithosphere. The low weight of lithospheric mantle underneath the Tibetan Plateau, however, does not correlate with thin lithospheric mantle.

GPE and force distributions for model 'Lithodens' depend on the mantle flow model and we again present results for our example model. The resulting GPE field (Fig. 5c) resembles that of model 'Crust2.0'. However, lateral variations are attenuated, mainly in southeast Asia and in the Atlantic. Generated forces are therefore considerably less chaotic.

4 TORQUE BALANCE ANALYSIS

We now proceed to evaluate whether our independent estimates of the various forces are consistent in that they balance the Eurasian Plate. We will show that this depends on the assumed mantle flow model. In this section, we concentrate on mantle flow models based on tomographic model 'ngrand'. First, we illustrate the torque balance analysis methodology by presenting results for our example mantle flow model. Subsequently, we investigate how torque results are affected by uncertainties in the conversion of seismic wave speed anomalies to density perturbations (v–ρ scaling) and the (radial) viscosity profile, and analyse how this affects the ability of mantle tractions to balance lithospheric forces on the Eurasian Plate. In Section 5 we subsequently analyse mantle flow models based on other mantle anomaly models.

4.1 Example mantle flow model

Shear resulting from active and passive mantle flow yields torques represented by the red star and square, respectively, in Fig. 2. The total mantle shear torque (red dot) is the sum of the two separate contributions and therefore lies on the connecting great-circle. Its location is closer to the active shear torque which is of higher magnitude than the passive shear torque. Torques resulting from the three LBF models (LBF torques, green triangles in Fig. 2) have quite similar orientations despite the differences in force pattern (Fig. 5). As concluded by WR10 for the case of isostatic models, the differences seen in force pattern occur on a small length scale compared to the plate size and cancel out upon integration. Torques for the isostatic models presented by WR10 are included for completeness in Fig. 2 (slightly altered due to update in some modelling parameters, black triangles).

To mechanically balance edge forces on Eurasia (eq. 1), mantle shear and LBFs must together produce a torque that is oriented inside the blue zone of Fig. 2 (see Section 2). This turns out to be the case for all three LBF models (blue crosses in Fig. 2). Tractions generated by our example mantle flow model thus balance lithospheric forces on Eurasia, indicating that independent estimates of edge forces and mantle tractions can indeed be reconciled into a total force set governing the dynamics of Eurasia. We proceed to evaluate the sensitivity of mantle flow models regarding their ability to balance Eurasia on the assumed mantle flow parameters.

4.2 Effect of v–ρ scaling factor

Conversion of seismic wave speed to density based on mineral physics laws is not straightforward as compositional and thermal effects are difficult to separate. Compositional effects are thought to be concentrated in the top part of the mantle, where cratonic roots are chemically distinct from the surrounding mantle (Jordan 1978; Forte & Perry 2000), and in the lowermost part of the mantle (Karato & Karki 2001; Steinberger & Holme 2008). It is therefore quite common in mantle flow modelling to assume a thermal origin for all anomalies and to use linear conversion between wave speed anomalies and densities. Most studies thereby remove density forcing in the top 200–300 km of the mantle to exclude the effect of cratonic roots (Lithgow-Bertelloni & Silver 1998; Becker & O'Connell 2001; Steinberger *et al.* 2001), where buoyancy variations due to temperature probably are largely cancelled by compositional variations (Forte & Perry 2000; Goes & van der Lee 2002). With the assumption of a thermal origin of all anomalies, v–ρ scaling factors for S-wave speeds have been estimated to lie between 0.10 and 0.30 (Karato & Karki 2001; Steinberger & Calderwood 2006; Simmons *et al.* 2009).

As a first-order approximation, we investigate the influence of uncertainties in v–ρ scaling on mantle tractions and resulting torques by assuming a constant scaling factor for the entire mantle, but removing forcing in the top 250 km. Active tractions magnitudes scale linearly with v–ρ scaling factor, whereas passive tractions are independent of mantle forcing and thus of v–ρ scaling. As a consequence, the relative contributions of active and passive shear to total mantle shear depends on the assumed v–ρ scaling. This is expressed in the orientation of the mantle shear torque, which location varies along the great-circle connecting the active and passive shear torques as a function of their relative magnitudes (Fig. 6). Mantle shear torque orientations for v–ρ scaling factors ranging between 0.10 and 0.30 form a 60° great-circle segment.

To evaluate the simplified v–ρ scaling adopted above, we compare results with torques obtained with (1) anomalies in the top 250 km of the tomographic model included and treated as fully thermal, (2) the use of the 1-D profile of Simmons *et al.* (2009; Fig. 7a), which has been developed through simultaneous inversion of tomographic and geodynamic models. This profile allows for variations of v–ρ scaling factor with depth, as would be expected in case of a depth-dependent compositional component in wave speed anomalies. We find torque orientations of active shear are slightly altered when the top 250 km of forcing is added to the mantle buoyancy field driving the flow. Total mantle shear torques for the assumed v–ρ scaling factor then form a segment along a slightly different great-circle, parallel to results for models without forcing in the top part of the mantle (Fig. 6). Results obtained with the depth-dependent scaling factor of Simmons *et al.* (2009) are in good agreement with the constant scaling factor results (red dot in Fig. 6). In accordance with Bull *et al.* (2010), the pattern of mantle flow thus seems relatively independent of v–ρ scaling. Overall, variations in mantle shear torque orientation perpendicular to the great-circle trend are largely inferior to variations parallel to it, and are thus dominated by the influence of v–ρ scaling on the relative magnitude of passive versus active shear. This effect is well captured by assuming a constant v–ρ scaling factor and varying its magnitude.

LBFs for models 'Mantle' and 'Lithodens' depend on the normal component of mantle tractions and are thus affected by the assumed v–ρ scaling. Torque results prove equally sensitive to the magnitude of v–ρ scaling factor as to whether or not the top 250 km is included in the forcing (Fig. 6). This is in accordance with Simmons *et al.* (2009), who showed dynamic topography to be particularly sensitive to lateral variations in v–ρ scaling factor for this top part of the Earth due to compositional effects. Sensitivity of the LBF torque to v–ρ scaling, however, is strongly inferior to that of the mantle shear torque, and is therefore unlikely to significantly influence the ability of a mantle flow model to balance Eurasia.

The dependence of torque results on v–ρ scaling has consequences for the possibility of torque balance on Eurasia, which is

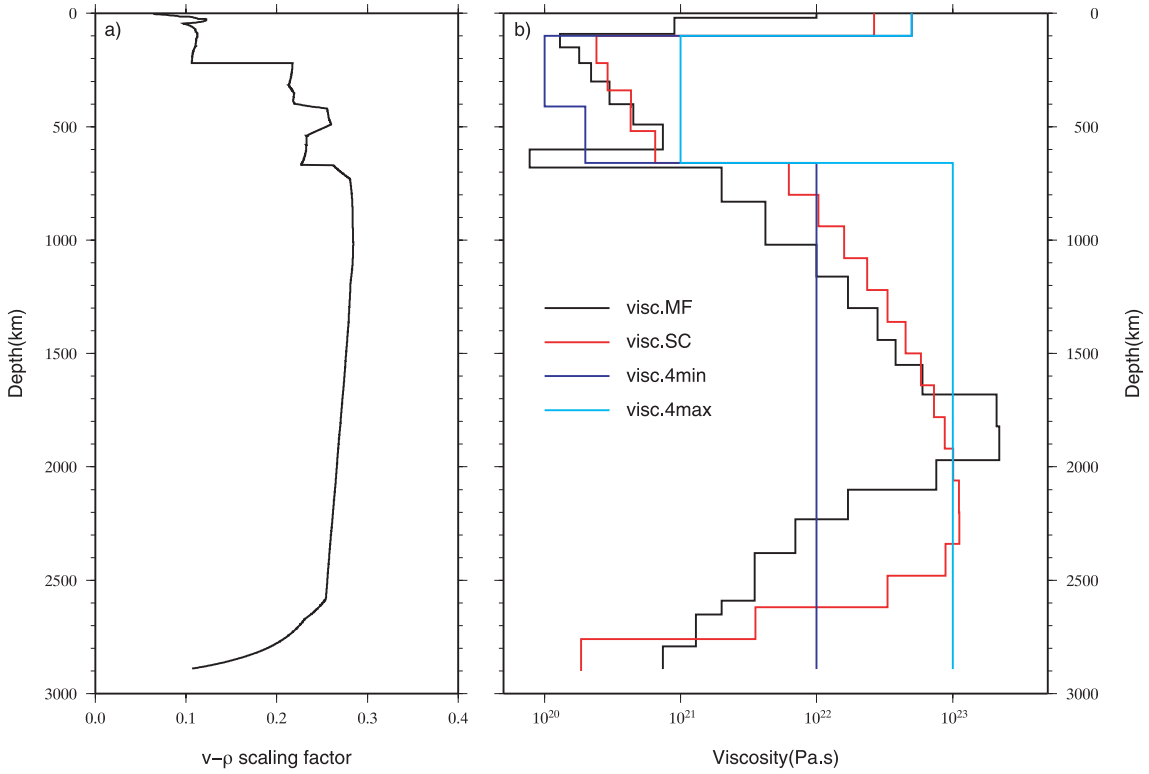

Figure 6. (a) Depth-dependent v–ρ scaling factor (Simmons *et al.* 2009). (b) Viscosity profiles used in this study. Key: visc.*MF* (Mitrovica & Forte 2004), visc.SC preferred profile (Steinberger & Calderwood 2006), visc.4min and visc.4max represent minimum and maximum values adopted in four-layer models, inferred from Steinberger & Calderwood (2006).

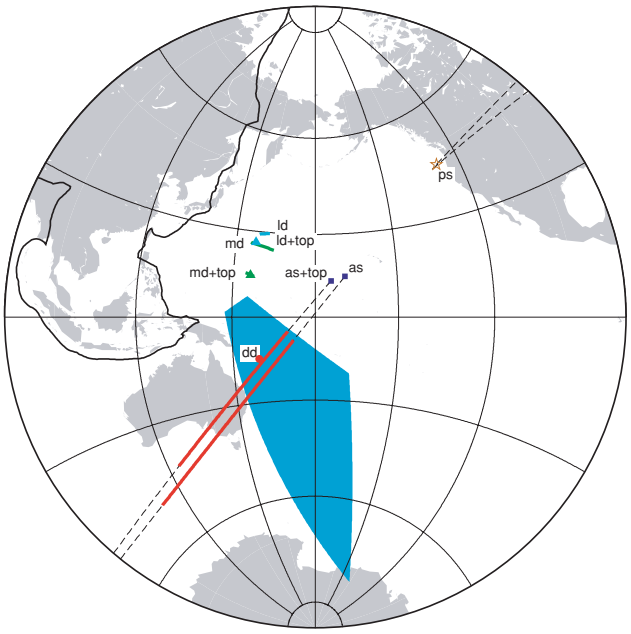

Figure 7. Sensitivity of mantle shear and LBF torque orientations to v–ρ scaling for tomographic model 'ngrand' and viscosity profile *MF*. Closed/open symbols represent the positive/negative end of torque vectors. For key see Table A2. +top stands for models including density forcing in top 250 km. Lines give torque orientation ranges for constant v–ρ scaling factor range of 0.10–0.30. Red dot, green/light blue triangles show results for depth-dependent (dd) scaling factor (Simmons *et al.* 2009).

only fulfilled for a particular range of v–ρ scaling factors. We find similar v–ρ scaling solution ranges for models in or excluding forcing in the top 250 km (Fig. 8). We also find that results do not significantly depend on the LBF model. Our results indicate that the simplification of a constant scaling factor is warranted for the purposes of this study, and that sensitivity to the top 250 km of forcing is limited. In our subsequent analysis we therefore represent the uncertainty in v–ρ scaling by varying the magnitude of a constant scaling factor and excluding the top 250 km of forcing.

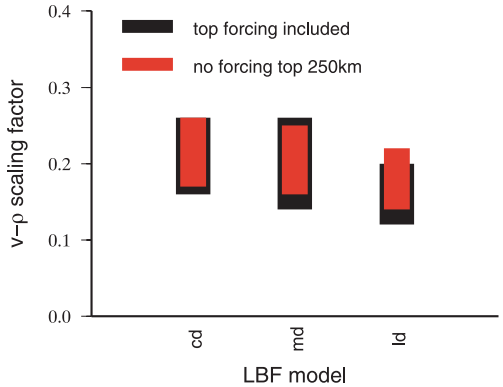

Figure 8. v–ρ scaling factor range producing mantle tractions that can balance the Eurasian Plate as a function of LBF model (tomographic model 'ngrand', viscosity profile *MF*). LBF models: see Table A2.

4.3 Effect of viscosity

Viscosity is an important parameter governing mantle flow, but still carries large uncertainties, both radially and laterally. In this study, we restrict ourselves to radially symmetric viscosity profiles, which allow for mantle flow calculations using a semi-analytic approach (see Section 8 for a discussion of possible implications of this assumption). We investigate the effect of mantle viscosity on torque results by working with two types of viscosity profiles. We use four-layer models, consisting of a lithosphere, upper mantle, transition zone and lower mantle, to systematically study the effect of variations in mantle viscosity. Dark and light blue lines in Fig. 7(b) represent the minimum and maximum values assumed for the different layers, which are inferred from Steinberger & Calderwood (2006). Furthermore, we use two radial viscosity profiles that were developed using geodynamic modelling and were shown to reproduce surface observables: profile *MF* (Mitrovica & Forte 2004), which we have used so far, and profile *SC* (Steinberger & Calderwood 2006, Fig. 7b).

Viscosity affects the flow response to buoyancy forces and to imposed plate motion differently and therefore influences the relative weight of active versus passive tractions generated by mantle flow (Behn *et al.* 2004; Naliboff *et al.* 2009). Active tractions result from Stokes flow and are therefore sensitive to viscosity distribution but not to the absolute viscosity value. Passive tractions, on the other hand, can be approximated by Couette flow, and depend on the absolute magnitude of viscosity. Shear torque results obtained with the four-layer viscosity models reflect these relations: the magnitude of the active shear torque is sensitive to the ratio of lower- and upper-mantle viscosity (Fig. 9a), whereas passive shear magnitudes are sensitive to upper-mantle viscosities (Fig. 9b). Scatter along the trends show second-order sensitivity to the viscosity of the transition zone. Passive shear magnitudes show a stronger dependence on viscosity than active shear so that the magnitude of the total mantle shear torque can approximately be related to the value of upper-mantle viscosity alone (Fig. 9c).

Torque orientations for passive and active shear (brown stars/blue squares in Fig. 10) vary slightly and moderately, respectively, as a function of viscosity profile, indicating that the pattern of mantle traction is also somewhat sensitive to viscosity. Orientations for total mantle shear torques vary strongly (red lines for v–ρ scaling factor range 0.10–0.30), reflecting the differences in ratio of passive and active shear torque magnitudes between models. The yellow zone in Fig. 10 is a schematic representation of the possible orientation of the total mantle shear torque for the four-layer viscosity models. Its elongated form following the great-circle trend connecting active and passive shear torques indicates that the dependence of mantle shear torque orientation on viscosity is dominated by the relative weight of the two contributions rather than by the pattern of the tractions. Results for the two more elaborate viscosity profiles *MF* and *SC* (thick lines in Fig. 10) are similar to the trend of the yellow zone and confirm this finding.

LBF torque orientations for model 'Mantle' and 'Lithodens' are somewhat sensitive to mantle viscosity (green and blue triangles, respectively, in Fig. 10 for v–ρ scaling factor of 0.30), but do not show the strong dependence displayed by the mantle shear torque. The effect of viscosity on the ability of mantle flow models to balance the Eurasian Plate is therefore mostly expressed through its influence on the torque magnitudes of passive and active shear. Because this effect is similar to that of v–ρ scaling (see Section 4.2) they can counterbalance each other. For every viscosity model a range of v–ρ scaling factors can be identified that allows for torque balance on Eurasia. We find that this range, which we will refer to as the torque balance solution range ('TBSR'), varies with the product of upper- and lower-mantle viscosity (Fig. 11). Results for the four-layer viscosity profiles (black, yellow and red stripes, depending on the LBF model used in the torque balance calculations) form a well-defined linear trend. Because all models are derived from the same tomographic model, v–ρ scaling factors yield a direct measure of the magnitude of the buoyancy forces that drive active mantle flow. Fig. 11 then visualizes a trade-off relation between viscosity and the magnitude of mantle buoyancy forces. The more viscous the mantle, the higher buoyancy forcing is required to balance Eurasia. A more viscous upper mantle increases passive shear, thus requiring stronger active flow to counteract its effect. A more viscous lower mantle is more difficult to bring into motion and requires higher forcing to generate the same amount of flow. Torque balance of Eurasia thus puts a strong constraint on the combination of mantle viscosity and the magnitude of mantle buoyancy forces.

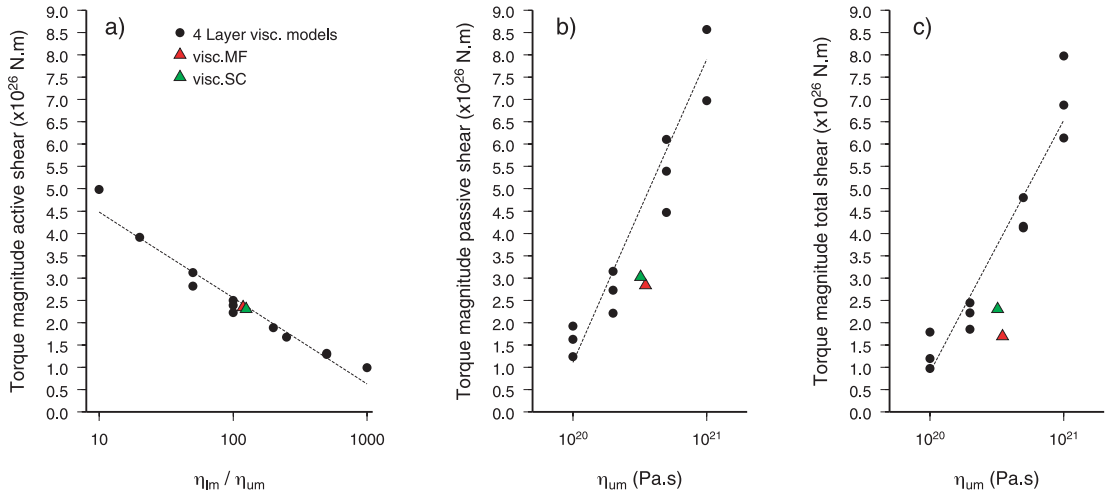

Figure 9. Dependence of torque magnitudes of (a) active shear, (b) passive shear and (c) total mantle shear on (average) viscosity of relevant layer (lm: lower mantle, um: upper mantle) for all considered viscosity profiles (see Fig. 7b). Scatter along trends show second-order sensitivity to the viscosity of the remaining layers. Results are shown for tomographic model 'ngrand' and v–ρ scaling of 0.20.

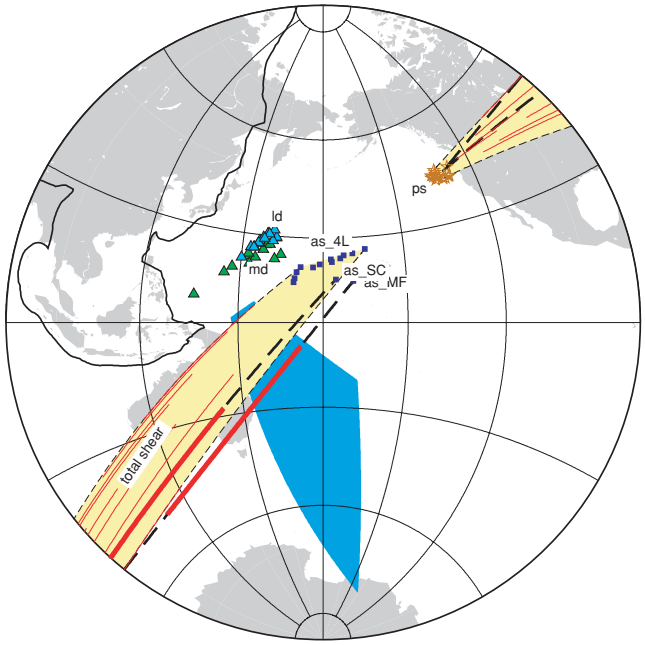

Figure 10. Sensitivity of mantle shear torque orientation to mantle viscosity structure for models based on tomographic model 'ngrand'. Brown stars: negative end of passive shear (ps), dark blue squares: active shear (as), red lines: total shear torque orientations for v–ρ scaling factors 0.10–0.30, green/light blue triangles: LBF model 'Mantle' (md)/'Lithodens'(ld). Four-layer viscosity profiles produce shear torque that fall into the yellow elongated zone. Key: 4*L*: four-layer viscosity profiles, *MF*: viscosity profile (Mitrovica & Forte 2004), *SC*: viscosity profile (Steinberger & Calderwood 2006).

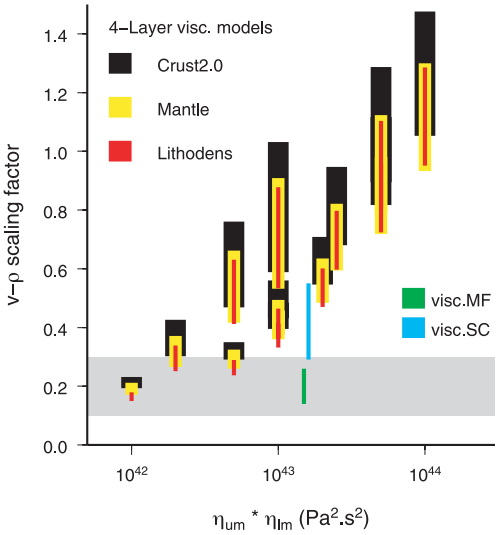

Figure 11. Torque balance solution range (TBSR) as a function of viscosity profile. For four-layer viscosity models results obtained using the three LBF models are presented separately; for viscosity profiles *MF* and *SC* the total range encompassing results for the three LBF models is given. Results are shown for tomographic model 'ngrand'. Realistic v–ρ scaling is indicated by grey range.

'TBSR' results show a similar trend for the three LBF models. Overall, slightly weaker mantle buoyancy forcing is required in case of LBF models 'Mantle' and 'Lithodens' than for model 'Crust2.0' (Fig. 11). These models include radial traction components from mantle flow models and the downhill forces caused by dynamic topography effectively amplify forcing due to active shear. The sensitivity of 'TBSR' results to the LBF model, however, is strongly inferior to the sensitivity to viscosity. Our conclusions regarding the ability of mantle flow models to balance Eurasia are therefore not affected by the choice of LBF model, and we conclude our results are independent of uncertainties regarding compensation of topography at depth. In our further analysis, we will therefore present 'TBSR' results that encompass the ranges for the three individual LBF models.

'TBSR' results for viscosity profiles *SC* and *MF* deviate from the trend of the four-layer viscosity models (Fig. 11). Although their averaged upper- and lower-mantle viscosities are relatively high, weak mantle buoyancy forcing is required for torque balance. Fig. 9 shows that active shear torque magnitudes for models *SC* and *FM* fit perfectly with the four-layer profiles trend, but passive shear torque magnitudes deviate significantly. Passive shear depends on the viscosity of the mantle just below the moving plates and is not well represented by average upper-mantle viscosities. Low asthenosphere viscosities in profile *MF*, and to some extent in profile *SC*, reduce passive shear relative to four-layer profiles with corresponding average upper-mantle viscosities. As a result, torque balance is achieved for lower active shear magnitudes, and thus lower v–ρ scaling factors. Although four-layer viscosity profiles give similar representation of active mantle flow than more elaborate depth-dependent viscosity profiles flow response to plate motion differs. Details of the viscosity profile in the uppermost mantle therefore have significant influence on the ability of a mantle flow model to balance the Eurasian Plate and need to be considered.

Overall, v–ρ scaling factors that balance Eurasia fall above the range proposed by mineral physics (grey band in Fig. 11) for most of the viscosity range. We find that for mantle flow models based on tomographic model 'ngrand' only weak rheologies produce flow that can be reconciled with Eurasian lithospheric dynamics. Partly, this can be attributed to the absence of a low-viscosity asthenosphere in the four-layer viscosity profiles. We will, however, show in the next section that this result also agrees with the low averaged anomaly magnitudes of tomographic model 'ngrand' relative to other models.

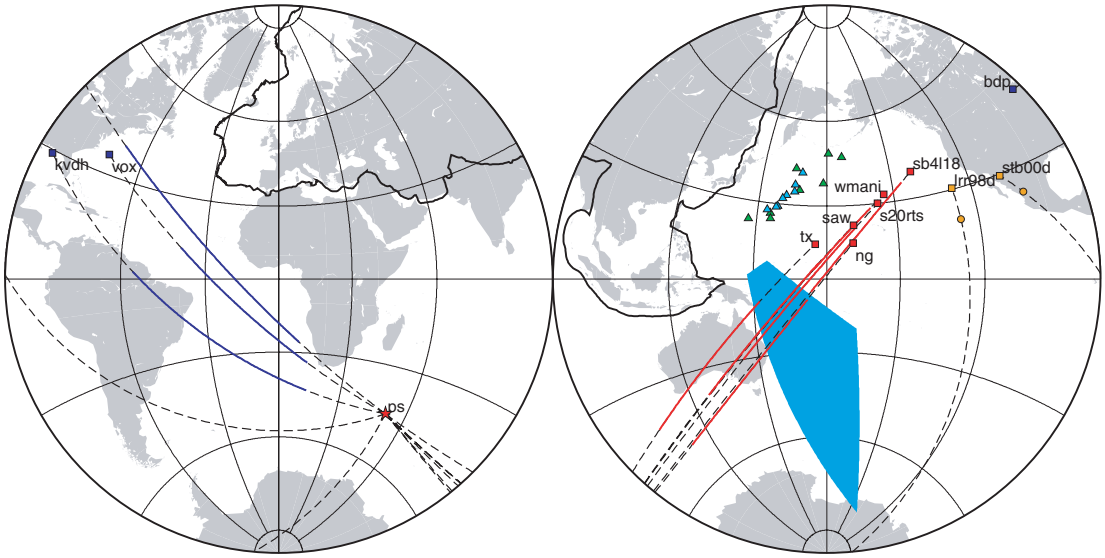

Figure 12. Torque orientations as a function of mantle anomaly model driving mantle flow for viscosity profile *MF*. Red/dark blue/orange: *S*-wave tomography/*P*-wave tomography/subduction-history models. Star: passive shear, squares: active shear, line/circles: total shear for constant v–ρ scaling factor of 0.10–0.30 (*S* wave), 0.20–0.60 (*P* wave) or no scaling (subduction-history). Green/light blue triangles: LBF model 'Mantle'/'Lithodens'. For key mantle anomaly models see text.

5 RESULTS AS A FUNCTION OF MANTLE ANOMALY MODEL

Tomographic studies have derived mantle velocity anomalies using different kinds of seismic measurements and techniques [review article: Romanowicz (2003)]. Although these models show considerable correlation on wavelength longer than 5000 km, they differ in their smaller scale features (Becker & Boschi 2002). Geodynamic density models derived from history of subduction are an alternative to tomographic models (Lithgow-Bertelloni & Richards 1998). These models lack contributions from upwelling material but have been shown to successfully reproduce plate motion (Becker & O'Connell 2001; Steiner & Conrad 2007).

Here, we evaluate mantle anomaly models on their ability to produce flow that can balance the Eurasian Plate. We analyse how mantle shear and LBF torques depend on the mantle anomaly model used to infer buoyancy forcing and investigate which mantle flow models meet the lithosphere-dynamics constraint outlined in Section 2. We incorporate our previous findings regarding the influence of v–ρ scaling and viscosity.

We consider six *S*-wave tomographic models [*S20RTS* (Ritsema & van Heijst 2000), *ng* (Grand 2002), *tx* (Simmons *et al.* 2007), *saw* (Megnin & Romanowicz 2000), *wmani* (Kustowski *et al.* 2008) and *sb2l18* (Masters *et al.* 2000)], three *P*-wave tomographic models [*kvdh* (Li *et al.* 2008), *vox* (Boschi *et al.* 2007) and *bdp* (Antolik *et al.* 2001)] and two geodynamic density models inferred from subduction history [*lrr98d* (Lithgow-Bertelloni & Richards 1998) and *stb00d* (Steinberger 2000)]. Tomographic models are converted to densities using a range of constant v–ρ scaling factors and excluding forcing in the top 250 km (Section 4.2). We will refer to resulting mantle shear torques by the name of the model used for density forcing. In accordance with our finding that details of viscosity distribution are significant (Section 4.3), we confine ourselves to viscosity profiles *MF* and *SC*.

Resulting torque orientations for viscosity profile *MF* are shown in Fig. 12. Results for viscosity profile *SC* show the same characteristics. Active shear torques on Eurasia differ considerably for the various models and group by origin type. This agrees with conclusions from Becker & Boschi (2002), who analysed various tomographic and subduction-history models and concluded that both *S*- and *P*-wave models show a higher level of correlation with members of their own type than with each other. Torque orientations for the subduction-history models compare significantly better to *S*- than *P*-wave models.

Total mantle shear torque orientations for each tomographic model are a linear combination of the corresponding active shear torque with the (model independent) passive shear torque, and vary along the connecting great-circles as a function of v–ρ scaling (Section 4.2). Subduction-history models directly describe density anomalies and should not require scaling. Results for *S*-wave tomographic models form a narrow band along the great-circle trend (Fig. 12), similar to results as a function of viscosity (Section 4.3). This reflects differences in anomaly magnitude of the various models; models generating stronger active tractions produce total shear torques that lie further away from the passive shear torque. The spread perpendicular to the great-circle is relatively small, indicating that uncertainties in shear pattern are of second order, at least for the long wavelengths to which torques are sensitive.

LBF torques for models 'Mantle' and 'Lithodens' (green/light blue triangles in Fig. 12) align along an elongated zone. The torque distribution as a function of mantle anomaly model shows similarity to that of the active shear torque. As highs in dynamic topography correspond to upwellings, around which flow is outwardly directed, and lows to downwellings, with inward directed flow, downhill forces due to dynamic topography tend to follow the same pattern as mantle shear.

Combining the above results with torques for edge forces (Section 2.2), we can assess the total torque on the Eurasian Plate as a function of mantle anomaly model, and evaluate for which models torque balance is achieved. We find that mantle flow models driven by *P*-wave anomalies cannot balance the Eurasian Plate, regardless of the magnitude of buoyancy anomalies (and thus of v–ρ scaling factor) or assumed viscosity profile. Our findings are similar to Becker & O'Connell (2001), who found that *P*-wave models lead to

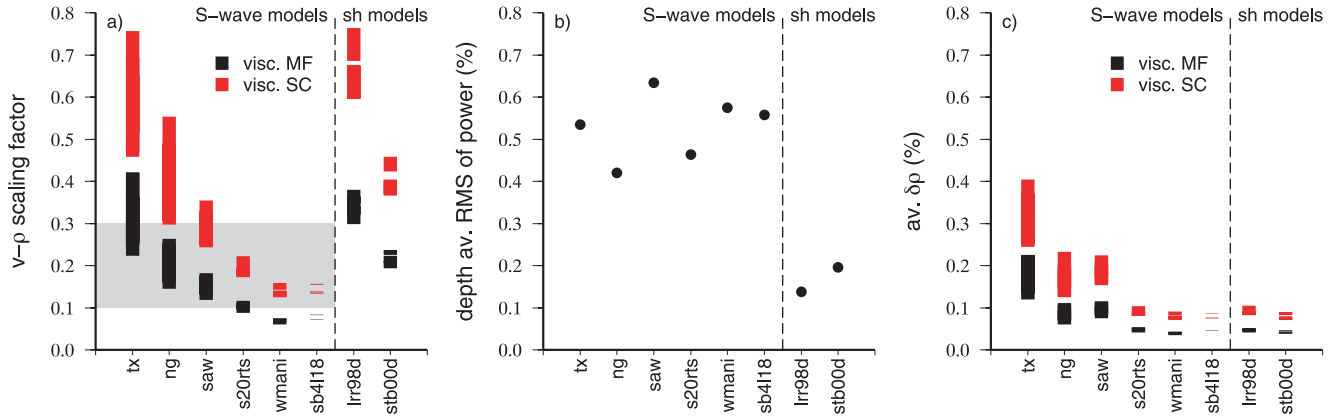

Figure 13. v–ρ scaling factor range (a) and buoyancy range (c) allowing for torque balance of Eurasia as a function of *S*-wave tomography model (presented ranges encompass results for the three LBF models). Subduction-history models (sh models) are included on the right-hand side of the graphs, the vertical bar in (a) in this case represents downscaling factors. Depth averaged rms of power of the various mantle anomaly models is given in (b). For key mantle anomaly and viscosity models see text.

bad predictions of plate velocities, unless combined with additional buoyancy forcing from upper-mantle slabs. The failure of *P*-wave models could be due to a lack of radial resolution in the upper mantle, causing seismically fast structures to mostly correlate with cratonic roots smeared out to great depth (Becker & O'Connell 2001; Becker & Boschi 2002). Additionally, our assumption of a constant scaling factor based on thermal origin of wave speed anomalies is likely to be inappropriate for *P* waves, which are particularly sensitive to compositional anomalies (Karato & Karki 2001).

The possibility of torque balance on Eurasia with mantle tractions driven by *S*-wave anomalies depends on viscosity and v–ρ scaling factor. For each *S*-wave tomographic model, torque balance of Eurasia is possible for a particular combination of viscosity and v–ρ scaling (Fig. 13a). Models with viscosity profile *SC*, which contains a stiffer asthenosphere, require higher v–ρ scaling factors than models with viscosity profile *MF*. The pattern as function of mantle anomaly model, however, is similar for both viscosity distributions. We find that all considered *S*-wave models can balance Eurasia in combination with v–ρ scaling magnitudes that fit estimates from mineral physics (grey range in Fig. 13a) for at least one of the two viscosity profiles.

Subduction-history models *lrr98d* and *stb00d* both generate active shear that is too dominant to fulfil the torque balance constraint. Assuming uncertainties in anomaly amplitudes are stronger than uncertainties in anomaly pattern, we have solved for a uniform scaling factor that downscales anomaly magnitudes to allow for torque balance. Results are presented alongside v–ρ scaling factors of *S*-wave models in Fig. 13(a).

The trade-off illustrated by Fig. 13(a) between mantle anomaly model and v–ρ scaling factor suggests that the main uncertainty due to mantle anomaly models arises from uncertainty in the magnitude of anomalies rather than in their pattern. This makes sense because tomography anomaly amplitudes are strongly affected by choices made regarding damping in the inversion. To assess whether this is truly the case, we compare the average anomaly magnitude of the different mantle anomaly models. Following Becker & Boschi (2002), we quantify the average magnitude of a tomographic/subduction-history model by the depth-averaged rms power of the spherical harmonic coefficients [Fig. 13b, for more detail see Becker & Boschi (2002)]. Multiplication of the depth average rms power with the applied v–ρ scaling factor then yields the average driving density anomaly (compared to Preliminary Reference Earth Model) for that specific mantle flow model.

Results for average density anomaly providing torque balance as a function of anomaly models are given in Fig. 13(c). We find that differences between models are indeed reduced after individual scaling from velocity to density. However, differences still persist. Model *tx* especially requires stronger density anomalies to balance Eurasia than other models on average. Because the effect of magnitude differences between models has been removed, remaining differences are caused by their specific patterns. Therefore, although uncertainty in mantle buoyancy pattern has a small effect on torque balance compared to uncertainty in buoyancy magnitude, we find it cannot be dismissed. Trade-off between mantle anomaly model and v–ρ scaling and/or viscosity is only partial. This implies that the choice for a specific anomaly model remains relevant for mantle flow calculations, not only on regional but also on plate-scale quantities.

In summary, we find that the mantle flow models based on *S*-wave tomographic models balance the Eurasian Plate for realistic viscosity profiles and v–ρ scaling. The subduction history models drive mantle flow that is too strong to fulfil the torque balance constraint, and can only balance Eurasia if downscaled. Mantle flow driven by a buoyancy field derived from the *P*-wave models produces tractions that do not balance the Eurasian Plate, regardless of viscosity or v–ρ scaling.

6 NATURE OF LITHOSPHERE–MANTLE COUPLING

The magnitude of active versus passive shear stresses at the base of the lithosphere indicates whether lithosphere–mantle coupling is dominated by drive from the mantle or from the plates. This ratio is not well constrained through mantle modelling alone, because it varies significantly depending on the assumed mantle buoyancy forcing and viscosity field. Fig. 14 shows that for the *S*-wave anomaly-based models considered in this study (all based on physically realistic v–ρ scaling and viscosity values) torque ratios of passive and active shear range between 0.25 and 2.7. Models thus vary between situations in which lithosphere–mantle interaction under Eurasia is governed almost entirely by plate motion or almost entirely by direct forcing from active mantle convection.

In the previous section, we have shown how uncertainties in mantle buoyancy and viscosity affect the ability of mantle flow to balance the Eurasian Plate through their effect on the relative

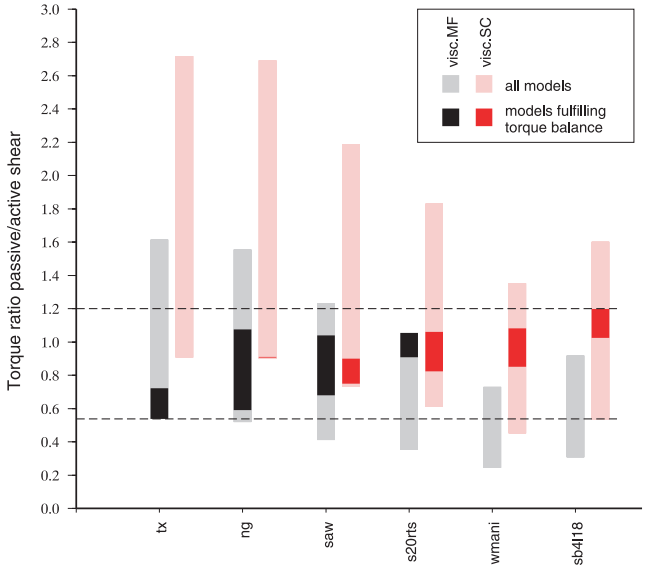

Figure 14. Torque magnitude ratio of passive and active shear for mantle flow models driven by *S*-wave anomalies. Shaded ranges shows values for all considered models (for physically realistic v–ρ scaling factor range of 0.10–0.30 and viscosity profiles *MF* and *SC*). Results for models fulfilling the torque balance constraint are shown in bright colours and constrain the passive/active shear ratio to values between 0.54 and 1.2. For key mantle anomaly an viscosity models see text.

magnitudes of active and passive shear stresses. Models that successfully balance Eurasia can therefore provide insight into the nature of lithosphere–mantle coupling. We find that successful models are all characterized by active/passive torque magnitude ratios between 0.54 and 1.2 (bright coloured selection in Fig. 14). The torque balance constraint thus considerably confines the relative importance of plate- versus mantle buoyancy-driven shear stresses under the Eurasian Plate. Balance occurs only if the contribution of passive shear to the dynamics of Eurasia is comparable to that of active shear. Because the active and passive shear torques are not antipodal (Fig. 12) their comparable magnitudes do not mean they entirely balance each other. The magnitudes of the total mantle shear torques (passive + active) are about half that of the two separate components, and require significant contributions from LBFs and edge force to be balanced (Section 7.1).

Our comparison of passive and active shear magnitudes is based on torques, which are integrated values over the area of the Eurasian Plate. Because the pattern of active shear is of considerably smaller wavelength than that of passive shear (Fig. 3), we find that locally, active shear stresses may be three to four times larger than passive shear stresses. Therefore, tractions at the base of the lithosphere are dominated by active mantle flow on a local scale, although tractions arising from resistance to plate motion are of the same importance on the plate scale.

Although Eurasian torque balance considerably confines the relative magnitudes of plate- and mantle buoyancy-driven shear stresses, some uncertainty remains because results depend on the tomographic model driving the flow (Fig. 14). As shown in Section 5, buoyancy magnitude differences between models can be compensated by adapting v–ρ scaling, but differences in the pattern of anomalies remain relevant. As a result, some scatter arises in the orientations of the active shear torques of the various models (Fig. 12). Models which active shear torques are located farther east require a relatively stronger passive shear component to balance Eurasia.

Our results indicate that the contribution to the dynamics of Eurasia of passive, plate motion-driven, shear stresses is comparable to that of active, mantle buoyancy-driven, shear. Active tractions are expected to be of similar magnitudes globe wide. Passive tractions, however, are mostly governed by the absolute velocity of the topping plate. Because Eurasia is a relatively slowly moving plate, we expect passive shear stresses under faster moving plates to be considerably stronger and therefore to dominate over active shear stresses. This could explain how the dynamics of certain plates could be successfully described including an approximation of mantle tractions as a uniform shear against the direction of absolute plate motion (Cloetingh & Wortel 1986; Wortel *et al.* 1991; Copley *et al.* 2010).

7 WHICH FORCES DRIVE EURASIA?

7.1 Relative importance of mantle shear, LBFs and edge forces

Our analysis provides a range of mechanically consistent sets of forces acting on the Eurasian Plate. This forms a strong physical basis to evaluate the role of different tectonic forces for the dynamics of Eurasia. We consider force sets including the different combinations of mantle flow and LBF models that have been shown to allow for torque balance (Section 5). Each combination thereby requires a specific balancing torque contribution from edge forces (one specific orientation located inside the red zone of Fig. 2). We note that because the system is underdetermined (seven unknown edge force magnitudes, three degrees of freedom), a specific edge force torque can result from different force distributions along the plate's boundary, which we do not specifically solve for.

We analyse the relative importance of mantle shear, LBFs and edge forces on Eurasia's dynamics by comparing the torque magnitudes of the individual force types with their scalar sum (the vector sum of the torques is implicitly zero because they form a balanced set). We find that results are very similar for all models: the edge force torque is consistently the strongest (Fig. 15). Edge forces account for almost half of the total torque magnitudes, regardless of the assumed mantle flow and LBF models. This is caused by the

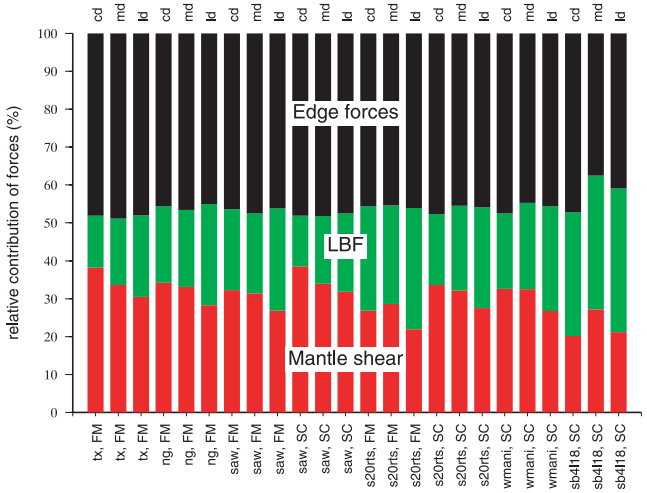

Figure 15. Relative magnitudes of mantle shear, LBF and edge forces torques for balancing forcing models (zero net torque), expressed as a percentage of their scalar sum. The lower horizontal axis specifies mantle flow model (tomographic model, viscosity profile, for key see text), upper axis specifies LBF model (key see Table A2).

torque's orientations (Fig. 2 and Fig. 12). For all models, orientations of mantle shear and LBF torques are considerably closer to each other than to the total edge force torque. Therefore their contributions add up constructively: $|\overline{T_{\rm ms}}| + |\overline{T_{\rm LBF}}| \sim |\overline{T_{\rm ms}} + \overline{T_{\rm LBF}}|$ and balancing edge forces hence contribute almost half of the total. The important role we find for edge forces in the dynamics of Eurasia agrees with results presented by Bird *et al.* (2008), who found that net edge force torques (referred to as side strength) are comparable to or stronger than mantle shear and LBF torques on most plates with large surface areas. The largest contribution to Eurasia's dynamics is thus provided by forces that are transmitted across plate boundaries.

The relative importance of mantle shear and LBFs is less well resolved because it depends on the assumed mantle flow and LBF models (Fig. 15). On average, the mantle shear torque is somewhat stronger, but we find mantle shear versus LBF torque magnitude distributions ranging from 75/25 per cent to 35/65 per cent. We note that forcing from mantle buoyancy forces underneath the lithosphere is represented in both terms: shear stresses contribute directly to the mantle shear torque whereas normal stresses affect LBFs. Generally, force models including dynamic topography directly from mantle flow modelling (based on LBF models 'Mantle' and 'Lithodens') have a relatively stronger LBF contribution than models that do not (based on LBF model 'Crust2.0'). As mentioned earlier, radial traction components in these models cause downhill forces that effectively amplify forcing due to active shear, thus requiring lower-mantle buoyancy forcing (and thus mantle shear) to balance the plate (Fig. 11). Our results encompass results found by different mantle convection-based studies. Neglecting dynamic topography, Becker & O'Connell (2001) found plates are driven for 70 per cent by mantle buoyancy forces and 30 per cent by LBFs, similar to earlier findings by Lithgow-Bertelloni & Richards (1998). Ghosh *et al.* (2008) pointed out that viscosity influences the relative strength of mantle shear and LBFs and found best matches to strain rate orientations for fifty-fifty forcing.

Overall, our analysis emphasizes the role of plate interaction in the mechanical balance of tectonic plates. Although our results regarding the relative weight of mantle shear and LBF are comparable to results from mantle convection-based studies, we find an additional and dominant net-contribution from edge forces is required to balance Eurasia. Implicitly imposing a zero net torque contribution from edge forces, common in global models that solve for plate velocities, may be inappropriate.

7.2 Eurasian Plate motion

The absolute motion of a plate is governed by the sum torque of the driving forces acting on it. With no significant slab pull and an averaged mantle shear not aligning with absolute plate motion (Warners-Ruckstuhl *et al.* 2010), identification of a main driving force for the Eurasian Plate is not straightforward. To assess which forces contribute to drive the plate, we compare our torque results with the orientation of the Euler pole of absolute plate motion. The sum torque of driving forces should parallel this Euler pole to drive Eurasia in the correct direction. Because our rheology lacks radial viscosity variations, net rotations of the lithosphere with respect to the mantle cannot be excited (O'Connell *et al.* 1991) and the no-net-rotation reference frame (Argus & Gordon 1991) is appropriate (for implications see Section 8).

A summary of our results for the orientation of the various model forces is displayed together with the Euler pole of absolute motion of Eurasia in Fig. 16. Ellipses represent the uncertainty range of the mantle flow-dependent forces. Only models that allow for torque balance are represented. The orientation of the Euler pole is not matched by one single torque and we cannot identify a single dominant driving force for Eurasia. Although the orientation of the active shear torque, which is the most prominent expression of mantle buoyancy forces, is consistent with that of a plate driving force, it does not explain observed plate motion on its own. As expected, passive shear is clearly a resistive force, with a torque orientation almost antipodal to absolute motion.

Gravitational forces acting directly on the Eurasian Plate are the most obvious driving forces. The sum torque of LBFs (including ridge push) and active shear is confined to orientations within the black shaded area in Fig. 16. Models based on realistic v–ρ scaling values (within the range suggested by mineral physics of 0.10–0.30) are restricted to the black area. The zones do not coincide with the Euler pole illustrating that the two forces do not collaborate to drive Eurasia in the observed direction. An additional force must therefore play a role. The plate's motion resulting from active shear and LBFs can be deviated towards the observed direction by a torque with an orientation inside the red shaded area of Fig. 16. The figure illustrates that such a torque arises from collision forces at Eurasia's southern boundary. We find either uniform collision forcing along the southern continental boundary, or a force distribution generating a similar torque but allowing for stronger collision along the Indian boundary, can push the plate towards its observed trajectory. This important role for edge forces in governing the absolute motion of Eurasia agrees with results presented by Iaffaldano & Bunge (2009), who found in a global analysis that a considerable part of total plate motion changes during the last 10 Myr could be explained by changes in force transmission across plate boundaries.

The observed direction of motion is only achieved for certain magnitudes of collision forces and thus provides a constraint on this magnitude. Depending on the mantle flow and LBF model we find that an average continental collision force of 2.7–5.0 $\times$ $10^{12}\,{\rm N\,m^{-1}}$ is required to match the observed motion direction, which is the equivalent of 27–50 MPa stress along a 100-km-thick boundary. Assuming contact area and forces to be twice as large on the collisional segment with India as on the rest of the boundary, we find force magnitudes of 4 to 6 and 2 to 3 $\times$ $10^{12}\,{\rm N\,m^{-1}}$, respectively, corresponding to stresses of 20 to 30 MPa. Those values agree with findings by Copley *et al.* (2010), who analysed the forces governing the dynamics of the Indian Plate and found collision forces on the contact with the Eurasian Plate of 5 to 6 $\times$ $10^{12}\,{\rm N\,m^{-1}}$. Becker & Faccenna (2011) recently proposed that strong active mantle tractions related to an active up-welling push the Arabian and Indian plates northwards. This could provide the engine behind the large collisional forces that we find are crutial to the dynamics of the Eurasian Plate.

8 MAIN UNCERTAINTIES

Finally, we consider the uncertainties that arise from assumptions made in the assessment of edge forces, LBFs and mantle tractions, and discuss how they may affect our conclusions.

8.1 Edge forces

The confinement of the orientation of the total edge force torque (red area in Fig. 2, which we will refer to as solution area) is crucial

for the resulting constraint on mantle forcing. We therefore evaluate how uncertainties in the modelling of edge forces may affect the orientation of the total edge force torque.

Our plate scale model is based on a simplified representation of the shape and nature of Eurasia's Plate boundaries. For each plate boundary type, we work with a net force that represents the sum of force contributions by processes at and beyond the domain boundaries. We solve for the average magnitude of this net force using torque balance. The direction of this net force varies with the location along the plate boundary. In our model, this direction is imposed based on the underlying force contribution that is deemed to be the most important. Different perspectives/choices are possible, and a main uncertainty thus arises from the direction of forcing imposed in the model. Below, we therefore evaluate changes in the solution area for the net edge force torque by assessing the sensitivity to alternative choices for all plate boundary types.

8.1.1 Roll-back margins

Roll-back margins are expected to be dominated by an outward pull perpendicular to the boundary from the retreating plate, but likely experience resistance at the plate contact antiparallel to the direction of relative plate motion. In the case of oblique subduction, which is common along Eurasia's boundaries, considerable resistance rotates the net forcing direction. Introducing resistance at roll-back margins in our model shifts the roll-back torque orientation southwards; in the extreme case of equal driving and resistive forcing magnitudes the torque shifts to a position close to the non-roll-back margins torque (Fig. 2). This effectively narrows the solution area of the total edge force. Because balance of mantle tractions and LBFs consistently requires an edge force torque oriented in the most southern part of the solution area, uncertainty in the direction of forcing at roll-back margins is not likely to affect our conclusions.

8.1.2 Continental collision and non-roll-back margins

Stress transmission along plate boundaries may differ between shear and normal components, potentially rotating resisting forces at collisional boundaries compared to our model that assumes them to be equal. We investigated the extreme case that only normal forces are transmitted through the plate contact. We found that, due to the geometry of the southern boundary of Eurasia in relation to the direction of absolute motion, the effect of variations in collision forcing is minimal after integration. The total continental collision torque (assuming equal forcing per metre boundary on the entire continental collision boundary) is shifted 10° westwards, only.

8.1.3 Transform boundaries

Transmission of normal stresses along transform boundaries would rotate forcing away from the imposed direction of shear. This force, usually referred to as transform push was neglected in our study. It has been shown not to influence the dynamics of the Juan da Fuca Plate (Govers & Meijer 2001). Adding a normal component at oceanic transform boundaries shifts the transform resistance torque northwards, potentially narrowing the edge force torque solution area at its southern boundary. However, its influence on the solution area is limited because continental collision forces also generate torques that lie in its southern part.

8.1.4 Continental boundary with North America

WR10 tested the sensitivity of the edge force solution area to boundary conditions on the unknown North America–Eurasia boundary segment and found the effect to be without significant consequences. Assuming that forces do not exceed the magnitudes along the remainder of the boundary, the orientation of the total continental collision torque shifts by a maximum of 10° when the North America–Eurasia boundary segment is added to it.

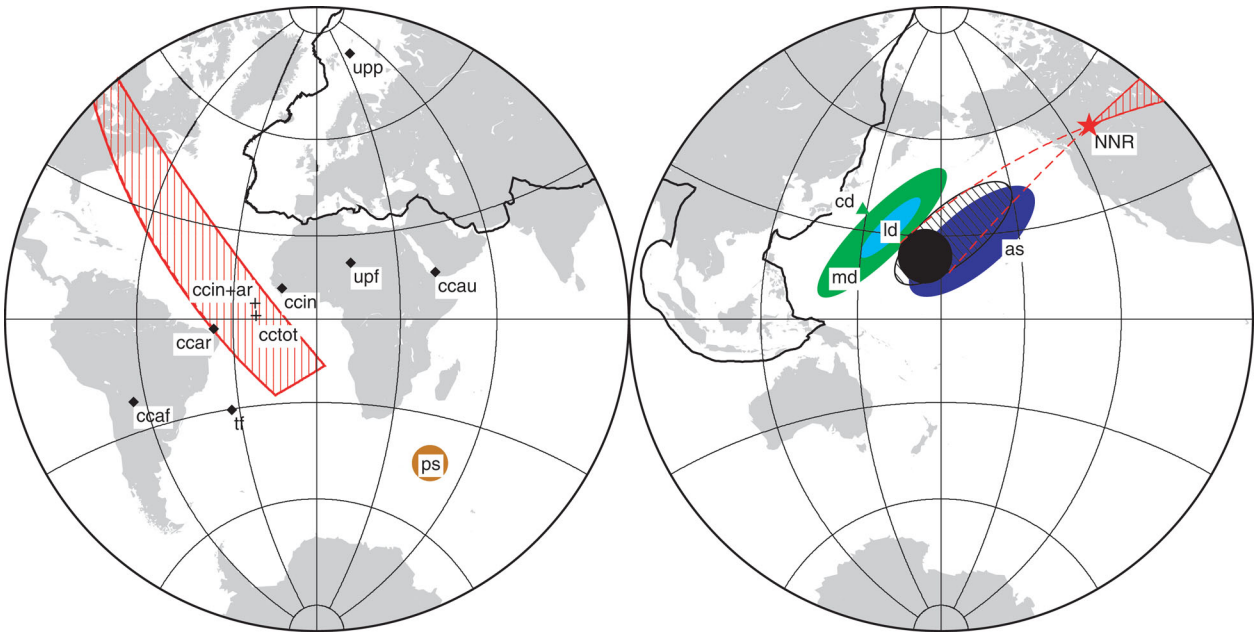

Figure 16. Analysis of plate driving forces. Torque orientations of the forces acting on the Eurasian Plate are compared to the Euler pole of absolute motion (Argus & Gordon 1991) (red star). Ellipses indicate uncertainty to mantle flow parameters for models that fulfil the torque balance constraint. Sum torques of active shear and LBFs generally fall into the shaded black ellipse, realistic models are confined to the black area. Red shaded area confines orientation of torques that can deviate the motion generated by active shear and LBFs towards the observed NNR motion. Continental collision on Eurasia's southern boundary complies. For key model forces see Table A2.

Torques of all edge forces may furthermore be affected by lateral variations in forcing, which are not taken into account in our simple parametrization, but may be considerable (Iaffaldano & Bunge 2009). We expect the largest lateral variations to occur along the continental collision contact, which accounts for the largest proportion of the boundary and where lateral variations in thickness of the plate contact are probable. We have therefore aimed to reduce the uncertainty that may arise from lateral forcing variations by allowing for different forcing magnitudes on continental collision segments as a function of the colliding plate. A test in which our different model forces were parametrized based on velocity-dependent forcing did not significantly alter the total edge force solution area, providing confidence that our conclusions are not too sensitive to the exact edge force distribution.

Due to the considerable uncertainties in assessing the imposed direction of forcing described, additional uncertainties in relative plate motion directions (DeMets *et al.* 1994) or exact plate boundary geometry are of second order and were not considered.

Overall, we conclude that local uncertainties in forcing affect the orientation of the total edge force torque only mildly and should not affect our conclusions regarding lithosphere–mantle coupling.

8.2 LBFs

By working with three LBF models, based on different assumptions regarding the compensation of topography at depth, we have aimed to cover the uncertainty range in LBFs on the Eurasian Plate. We realize this aim may not be fully achieved; especially the treatment of lateral variations in lithospheric mantle properties may have important effects that were not considered (Pascal 2006). However, although the three models considered produce quite different force fields, their differences occur on small length scales compared to the plate's size and only mildly affect the resulting torque on Eurasia. This indicates the LBF torque on Eurasia is well constrained.

8.3 Mantle flow modelling

Our mantle flow calculations do not include LVVs. The role of LVVs on mantle flow and tractions at the base of the lithosphere has been extensively investigated in recent years (Becker 2006; Conrad & Lithgow-Bertelloni 2006; Moucha *et al.* 2007; Ghosh *et al.* 2010); for a review see Becker & Faccenna (2009). Viscosity variations of around one order of magnitude underneath oceanic and continental regions and stiff cratonic roots reaching up to 400 km depth have been shown to have an important effect on mantle dynamics in that they generate net rotation of the lithosphere (Zhong 2001; Becker 2006), absent in mantle flow calculations lacking LVVs. Several studies, however, have indicated that the effect of LVVs on the generated flow field may be restricted (Becker 2006; Moucha *et al.* 2007). Conrad & Lithgow-Bertelloni (2006) explicitly analysed the effect of LVVs in the uppermost mantle on excited tractions at the base of the lithosphere and found that the direction of shear varies little, although amplitudes scale with the viscosity increase at continental roots. Becker (2006) concludes that mantle flow models with prescribed plate motions result in similar flow fields in models with and without LVVs if the appropriate net rotation of the lithosphere with respect to the lower mantle is taken into account, and that LVVs only play a minor role in large-scale features.

Since our analysis concerns plate-scale quantities, the main uncertainty in our modelled mantle tractions likely results from neglecting net rotation of the lithosphere. Lithospheric net rotation has been estimated based on hotspot tracks (Gordon & Jurdy 1986; Wang & Wang 2001; Gripp & Gordon 2002; Steinberger *et al.* 2004; O'Neill *et al.* 2005; Torsvik *et al.* 2010), mantle flow modelling (Zhong 2001; Becker 2006) and anisotropic constraints (Kreemer 2009; Conrad & Behn 2010) and consistently indicates a westward drift of the lithosphere. Although the magnitude of rotation remains uncertain, recent estimates all suggest a relatively slow rotation of 0.1° to $0.2^\circ\,\mathrm{Myr}^{-1}$ (Conrad & Behn 2010; Torsvik *et al.* 2010). With Eurasia also moving slowly ($0.24^\circ\,\mathrm{Myr}^{-1}$ in the NNR reference frame), net rotation can potentially have a considerable effect on passive tractions at the base of the plate.

The Euler pole of lithospheric net rotation is approximately opposite to the pole of absolute motion of Eurasia in an NNR reference frame (Fig. 17). Therefore, any net rotation effectively decreases Eurasia's absolute motion without affecting its direction. Because passive tractions mainly result from resistance against motion of the Eurasian Plate itself (see Fig. 3b), we expect net rotation to simply reduce their magnitudes. Balance of the Eurasian Plate requires a specific ratio of passive and active tractions (Section 5), which means that active traction magnitudes required to balance the plate will scale accordingly. Net rotation will thus affect the absolute magnitude of mantle tractions but not their directions or the relative importance of active versus passive shear. Because net rotation decreases the magnitude of the mantle shear torque it reduces its share in the total dynamics of Eurasia to the advantage of LBFs. The magnitude of the edge force torque is determined by the sum of the mantle shear and LBF torques; hence, its relative contribution is preserved. We conclude that our results regarding the nature of lithosphere–mantle coupling and the relative importance of edge forces to the dynamics of Eurasia are rather insensitive to net rotation of the lithosphere. Our results for the absolute magnitude of balancing mantle tractions, however, are likely to decrease as a function of net rotation and should be regarded as upper limits.

9 CONCLUSIONS

We use mechanical equilibrium of Eurasia to analyse tractions arising from global convective mantle flow models in the light of lithospheric dynamics. We show that current modelling approaches of lithosphere dynamics and mantle flow can successfully be integrated into a new, single-plate scale, combined approach. Results obtained through this combined approach, some new and others confirming earlier results, have the added value of the more complete approach. Our analysis yields a range of mechanically consistent sets of forces acting on the Eurasian Plate, which provide insight in the role of the different forces in the dynamics of Eurasia. We conclude that:

(i) Of the explored set of mantle anomaly models, mantle flow models based on *S*-wave tomography produce mantle tractions that meet the torque balance constraint for realistic radial viscosity profiles and v–ρ scaling. Subduction history models drive mantle flow that is too strong to fulfil the torque balance constraint, and can only balance Eurasia if downscaled. Mantle flow driven by a buoyancy field derived from *P*-wave anomalies produces tractions that do not balance the Eurasian Plate, regardless of viscosity or v–ρ scaling.

(ii) Torque balance can only be achieved in case torques arising from passive (i.e. plate motion driven) and active (i.e. mantle buoyancy driven) shear are of similar magnitudes. Therefore, we conclude that lithosphere–mantle coupling is equally governed by resistance to plate motion as by active forcing from the underlying mantle. On a local scale, however, tractions at the base of the

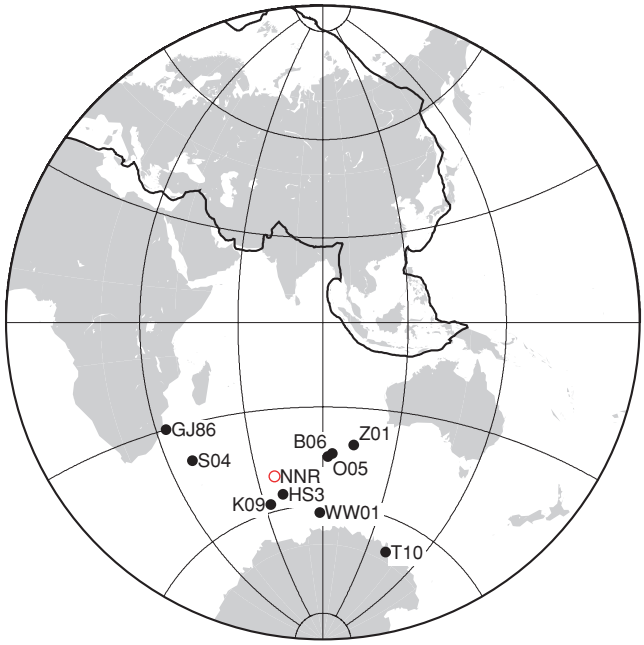

Figure 17. Net-rotation Euler poles from various studies as reported by Conrad & Behn (2010) [black dots: GJ86 (Gordon & Jurdy 1986), HS3 (Gripp & Gordon 2002), WW01 (Wang & Wang 2001), Z01 (Zhong 2001), S04 (Steinberger *et al.* 2004), O05 (O'Neill *et al.* 2005), B06 (Becker 2006), K09 (Kreemer 2009) and T10 (Torsvik *et al.* 2010)]. The red circle represents the negative end of the Euler pole vector of absolute motion of Eurasia in an NNR reference frame (NNR, Argus & Gordon 1991).

lithosphere are dominated by active mantle flow due to their short wavelength character. Although the two shear contributions produce torques of similar magnitudes they do not balance each other.

(iii) A considerable net torque from edge forces is required to balance total mantle tractions and LBFs. This torque is stronger than the mantle and LBFs torques regardless of considered uncertainties. Hence, the largest contribution to Eurasia's dynamics is provided by forces originating on other plates and transmitted across plate boundaries. This result suggests that implicitly imposing a zero net torque contribution from edge forces, common in global models that solve for plate velocities, is inappropriate.

(iv) Our torque analysis shows that the largest uncertainties in mantle tractions at the base of the lithosphere arise from differences in flow magnitude rather than pattern between mantle flow models. Anomaly magnitudes in the tomographic/subduction history models, velocity–density scaling and viscosity all influence the relative magnitude of passive versus active tractions under the lithosphere, which is the key factor in fulfilling Eurasian torque balance. However, differences in mantle buoyancy patterns do remain significant and trade-off with v–ρ scaling and/or viscosity is only partial. Our results do not significantly depend on uncertainties regarding compensation of topography with depth.

(v) Although mantle flow and LBFs are the main drivers of Eurasia's absolute motion, continental collision at Eurasia's southern boundary significantly contributes by pushing the plate northwards. Depending on the assumed mantle flow parameters, averaged collision forces along the southern boundary of $2.7–5.0 \times 10^{12}$ N m^{-1} are required to match the observed direction of motion.

ACKNOWLEDGMENTS

We thank Gene Humphreys and editor Bruce Buffet for their stimulating remarks, which helped improve the manuscript, as well as Thorsten Becker for enlightening discussions and comments on an earlier draft, Nathan Simmons for discussions on velocity–density scaling and Bernhard Steinberger for discussion on mantle tractions in an early stage of this work. This manuscript has also benefited from careful reviews by Lucy Flesh and Greg Houseman as part of the evaluation of KWR's thesis. Figures were produced with the GMT software by Wessel & Smith (1991). Work was supported by the Netherlands Organisation for Scientific Research (NWO, Earth and Life Sciences (ALW)), in the context of the EUROMARGINS EUROCORES Programme of the European Science Foundation, project 01-LEC-EMA22F WESTMED.

REFERENCES

Amante, C. & Eakins, B.W., 2009. ETOPO1 1 arc-minute global relief model: Procedures, data sources and analysis. NOAA Technical Memorandum NESDIS NGDC-24, p. 19.

Antolik, M., Ekstrom, G. & Dziewonski, A.M., 2001. Global event location with full and sparse data sets using three-dimensional models of mantle P-wave velocity, *Pure appl. Geophys.,* **158,** 291–317.

Argus, D.F. & Gordon, R.G., 1991. No-net-rotation model of current plate velocities incorporating plate motion model NUVEL-1, *Geophys. Res. Lett.,* **18,** 2039–2042.

Artemieva, I.M., 2003. Lithospheric structure, composition, and thermal regime of the east European craton: implications for the subsidence of the Russian platform, *Earth planet. Sci. Lett.,* **213,** 431–446.

Artemieva, I.M., 2006. Global 1° × 1° thermal model TC1 for the continental lithosphere: implications for lithosphere secular evolution, *Tectonophysics,* **216,** 245–277.

Artyushkov, E.V., 1973. Stresses in the lithosphere caused by crustal thickness inhomogeneities, *J. geophys. Res.,* **78,** 7675–7708.

Bassin, C., Laske, G. & Masters, G., 2000. The current limits of resolution for surface wave tomography in North America, *EOS, Trans. Am. geophys. Un.,* **81,** F897.

Becker, T.W., 2006. On the effect of temperature and strain-rate dependent viscosity on global mantle flow, net rotation and plate-driving forces, *Geophys. J. Int.,* **167,** 943–957.

Becker, T.W. & Boschi, L., 2002. A comparison of tomographic and geodynamic mantle models, *Geochem. Geophys. Geosyst.,* **3,** doi:10.1029/2001GC000168.

Becker, T.W. & Faccenna, C., 2009. A review on the role of subduction dynamics for regional and global plate motion, in *Subduction Zone Geodynamics,* pp. 3–34, Springer, Berlin.

Becker, T.W. & Faccenna, C., 2011. Mantle conveyor beneath the Tethyan collisional belt, *Earth planet. Sci. Lett.,* **310**(3), 453–461.

Becker, T.W. & O'Connell, R.J., 2001. Predicting plate velocities with mantle circulation models, *Geochem. Geophys. Geosyst.,* **2,** doi:10.1029/2001GC000171.

Becker, T.W., Conrad, C., Lithgow-Bertelloni, C., O'Connell, R., O'Neill, C., Richards, M., Steinberger, B. & Zhong, S., 2006. Global spectral flow code development and benchmark plan. Available at: http://geosys.usc.edu/projects/seatree (last accessed 2011 June).

Behn, M.D., Conrad, C.P. & Silver, P.G., 2004. Detection of upper mantle flow associated with the African superplume, *Earth planet. Sci. Lett.,* **224**(3–4), 259–274.

Bird, P., 2003. An updated digital model of plate boundaries, *Geochem. Geophys. Geosyst.,* **4,** doi:10.1029/2001GC000252.

Bird, P., Liu, Z. & Rucker, W.K., 2008. Stresses that drive the plates from below: definitions, computational path, model optimization and error analysis, *J. geophys. Res.,* **113,** doi:10.1029/2007JB005460.

Boschi, L., Becker, T.W. & Steinberger, B., 2007. Mantle plumes: dynamic models and seismic images, *Geochem. Geophys. Geosyst.,* **8,** doi:10.1029/2007GC001733.

Bull, A.L., McNarama, A.K., Becker, T.W. & Ritsema, J., 2010. Global scale model of the mantle flow field predicted by synthetic tomography models, *Phys. Earth planet. Inter.,* **182,** 129–138.

Čadek, O. & Fleitout, L., 1999. A global geoid model with imposed plate velocities and partial layering, *J. geophys. Res.,* **104,** 29055–29075.

Chapple, W.M. & Tullis, T.E., 1977. Evaluation of the forces that drive the plates, *J. geophys. Res.,* **82,** 1967–1984.

Cloetingh, S. & Wortel, R., 1986. Stress in the Indo Australian plate, *Tectonophysics,* **132**(1–3), 49–67.

Conrad, C.P. & Behn, M.D., 2010. Constraints on lithosphere net rotation and asthenospheric viscosity from global mantle flow models and seismic anisotropy, *Geochem. Geophys. Geosyst.,* **11,** doi:10.1029/2009GC002970.

Conrad, C.P. & Lithgow-Bertelloni, C., 2002. How mantle slabs drive plate tectonics, *Science,* **298,** 207–209.

Conrad, C.P. & Lithgow-Bertelloni, C., 2004. The temporal evolution of plate driving forces: importance of slab suction versus slab pull during the cenozoic, *J. geophys. Res.,* **109,** doi:10.1029/2004JB002991.

Conrad, C.P. & Lithgow-Bertelloni, C., 2006. Influence of continental roots and asthenosphere on plate-mantle coupling, *Geophys. Res. Lett.,* **33**(5), doi:10.1029/2005GL025621.

Conrad, C.P., Lithgow-Bertelloni, C. & Louden, K.E., 2004. Iceland, the Faralon slab, and dynamic topography of the north Atlantic, *Geology,* **32,** 177–180.

Copley, A., Avouac, J.P. & Royer, J.Y., 2010. India-Asia collision and the Cenozoic slowdown of the Indian plate: implications for the forces driving plate motions, *J. geophys. Res.,* **115,** doi:10.1029/2009JB006634.

Crough, S.T., 1975. Thermal model of oceanic lithosphere, *Nature,* **256,** 388–390.

DeMets, C., Gordon, R.G., Argus, D.F. & Stein, S., 1994. Effect of recent revisions to the geomagnetic reversal time scale on estimates of current plate motion, *Geophys. Res. Lett.,* **21,** 2191–2194.

Fleitout, L. & Froidevaux, C., 1982. Tectonics and topography for a lithosphere containing density heterogeneities, *Tectonics,* **1,** 21–56.

Flesch, L.M., Holt, W.E., Haines, A.J., Wen, L. & Shen-Tu, B., 2007. The dynamics of western North America: stress magnitudes and the relative role of gravitational potential energy, plate interaction at the boundary and basal tractions, *Geophys. J. Int.,* **169**(3), 866–896.

Forsyth, D.W. & Uyeda, S., 1975. On the relative importance of the driving forces of plate motion, *Geophys. J. R. astr. Soc.,* **43,** 163–200.

Forte, A.M. & Perry, C.H.K., 2000. Geodynamic evidence for a chemically depleted continental tectosphere, *Science,* **290,** doi:10.1126/science.290.5498.1940.

Forte, A.M., Moucha, R., Simmons, N.A., Grand, S.P. & Mitrovica, J.X., 2010. Deep-mantle contributions to the surface dynamics of the North American continent, *Tectonophysics,* **481,** 3–15.

Ghosh, A., Holt, W.E., Wen, L., Haines, A.J. & Flesch, L.M., 2008. Joint modeling of lithosphere and mantle dynamics elucidating lithosphere-mantle coupling, *Geophys. Res. Lett.,* **35,** doi:10.10292008GL034365.

Ghosh, A., Holt, W.E. & Flesch, L.M., 2009. Contribution of gravitational potential energy differences to the global stress field, *Geophys. J. Int.,* **179,** 787–812.

Ghosh, A., Becker, T.W. & Zhong, S.J., 2010. Effects of lateral viscosity variations on the geoid, *Geophys. Res. Lett.,* **37,** doi:10.1029/2009GL040426.

Goes, S. & van der Lee, S., 2002. Thermal structure of the North American uppermost mantle inferred from seismic tomography, *J. geophys. Res.,* **107,** doi:10.1029/22000JB000049.

Goes, S., Loohuis, J.J.P., Wortel, M.J.R. & Govers, R., 2000. The effect of plate stresses and shallow mantle temperatures on tectonics of north western Europe, *Global Planet. Change,* **27,** 23–38.

Gordon, R.G. & Jurdy, D.M., 1986. Cenozoic global plate motions, *J. geophys. Res.,* **91,** 12 389–12 406.

Govers, R. & Meijer, P.T., 2001. On the dynamics of the Juan de Fuca plate, *Earth planet. Sci. Lett.,* **189,** 115–131.

Grand, S.P., 2002. Mantle shear wave tomography and the fate of subducted slabs, *Phil. Trans. R. Soc. Lond,* **360,** 2475–2491.

Gripp, A.E. & Gordon, R.G., 2002. Young tracks of hotspots and current plate velocities, *Geophys. J. Int.,* **150,** 321–361.

Hager, B.H. & O'Connell, R.J., 1981. A simple global model of plate dynamics and mantle convection, *J. geophys. Res.,* **86,** 4843–4867.

Hager, B.H., Clayton, R.W., Richards, M.A., Comer, R.P. & Dziewonski, A.M., 1985. Lower mantle heterogeneity, dynamic topography and the geoid, *Nature,* **113,** 541–545.

Harper, J.F., 1975. On the driving forces of plate tectonics, *Geophys. J. R. astr. Soc.,* **40**(3), 465–474.

Humphreys, E.D. & Coblentz, D.D., 2007. North American dynamics and western US tectonics, *Rev. Geophys.,* **45,** 8755–1209.

Iaffaldano, G. & Bunge, H.P., 2009. Relating rapid plate-motion variations to plate-boundary forces in global coupled models of the mantle/lithosphere system: effects of topography and friction, *Tectonophysics,* **474,** 393–404.

Jordan, T.H., 1978. Composition and development of the continental tectosphere, *Nature,* **274,** 544–548.

Karato, S.I. & Karki, B.B., 2001. Origin of lateral variation of seismic wave velocities and density in the deep mantle, *J. geophys. Res.,* **106,** 21 771–21 783.

Karpychev, M. & Fleitout, L., 1996. Simple considerations on forces driving plate motion and on the plate-tectonic contribution to the long-wavelength geoid, *Geophys. J. Int.,* **127**(2) 268–282.

Kreemer, C., 2009. Absolute plate motions constrained by shear wave splitting orientations with implications for hot spot motions and mantle flow, *J. geophys. Res.,* **114,** doi:10.1029/2009JB006416.

Kustowski, B., Ekstrom, G. & Dziewonski, A.M., 2008. Anisotropic shear-wave velocity structure of the Earth's mantle: a global model, *J. geophys. Res.,* **113,** doi:10.1029/2007JB005169.

Li, C., van der Hilst, R.D., Engdahl, E.R. & Burdick, S., 2008. A new global model for P wave speed variations in Earth's mantle, *Geochem. Geophys. Geosyst.,* **9**(5), doi:10.1029/2007GC001806.

Lister, C. R.B., 1975. Gravitational drive on oceanic plates caused by thermal contraction, *Nature,* **257,** 663–665.

Lithgow-Bertelloni, C. & Guynn, J.H., 2004. Origin of the lithospheric stress field, *J. geophys. Res.,* **109,** doi:10.1029/2003JB002467.

Lithgow-Bertelloni, C. & Richards, M.A., 1998. The dynamics of Cenozoic and Mesozoic plate motions, *Rev. Geophys.,* **36,** 27–78.

Lithgow-Bertelloni, C. & Silver, P.G., 1998. Dynamic topography, plate driving forces and the African superswell, *Nature,* **395,** 269–272.

Liu, Z. & Bird, P., 2002. North America plate is driven westward by lower mantle flow, *Geophys. Res. Lett.,* **29,** doi:10.1029/2002GL016002.

Masters, G., Laske, G., Bolton, H. & Dziewonski, A., 2000. The relative behavior of shear velocity, bulk sound speed, and compressional velocity in the mantle: implications for chemical and thermal structure, *Am. geophys. Un. Monograph,* **117,** 63–88.

Megnin, C. & Romanowicz, B., 2000. The shear velocity structure of the mantle from the inversion of body, surface and higher modes waveforms, *Geophys. J. Int.,* **143,** 709–728.

Meier, U., Curtis, A. & Trampert, J., 2007. Fully nonlinear inversion of fundamental mode surface wave for a global crustal thickness model, *Geophys. Res. Lett.,* **34,** doi:10.1029/2007GL030989.

Meijer, P.T. & Wortel, M.J.R., 1992. The dynamics of motion of the South American plate, *J. geophys. Res.,* **97,** 11 915–11 931.

Milner, K., Becker, T.W., Boschi, L., Sain, J., Schorlemmer, D. & H., W., 2009. The solid earth research and teaching environment: a new software framework to share research tools in the classroom and across disciplines, *EOS, Trans. Am. geophys. Un.,* **90,** 104.

Mitrovica, J.X. & Forte, A.M., 2004. A new inference of mantle viscosity based upon joint inversion of convection and glacial isostatic adjustment data, *Earth planet. Sci. Lett.,* **225,** 177–189.

Molnar, P. & Lyon-Cean, H., 1988. Some simple physical aspects of the support, structure, and evolution of mountain belts, *Spec. Pap. Geol. Soc. Am.,* **218,** 179–207.

Moucha, R., Forte, A.M., Mitrovica, J.X. & Daradich, A., 2007. Lateral variations in mantle rheology: implications for convection related surface observables and inferred viscosity models, *Geophys. J. Int.,* **169**(1), 113–135.

Müller, R., Sdrolias, M., Gaina, C. & Roest, W.R., 2008. Age, spreading rates, and spreading asymmetry of the world's ocean crust, *Geochem. Geophys. Geosyst.,* **9,** doi:10.1029/2007GC001743.

Naliboff, J.B., Conrad, C.P. & Lithgow-Bertelloni, C., 2009. Modification of the lithospheric stress field by lateral variations in plate-mantle coupling, *Geophys. Res. Lett.,* **36,** doi:10.1029/2009GL040484.

O'Connell, R.J., Gable, C.W. & Hager, B.H., 1991. Toroidal-poloidal partitioning of lithospheric plate motions, in *Sea-Level and Mantle Rheology,* pp. 535–551, Kluwer Academic, Dordrecht.

O'Neill, C., Müller, R.D. & Steinberger, B., 2005. On the uncertainties in hot spot reconstructions and the significance of moving hot spot reference frames, *Geochem. Geophys. Geosyst.,* **6,** doi:10.1029/2004GC000784.

Panasyuk, S.V. & Hager, B.H., 2000. Models of isostatic and dynamic topography, geoid anomalies, and their uncertainties, *J. geophys. Res.,* **105,** 28 199–28 209.

Pascal, C., 2006. On the role of heat flow, lithosphere thickness and lithosphere density on gravitational potential stresses, *Tectonophysics,* **425**(1–4), 83–99.

Ricard, Y. & Vigny, C., 1989. Mantle dynamics with induced plate tectonics, *J. geophys. Res.,* **94**(B12), 17543–17560.

Richardson, R.M., Solomon, S.C. & Sleep, N.H., 1979. Tectonic stress in the plates, *Rev. Geophys.,* **17,** 981–1019.

Ritsema, J. & van Heijst, H.J., 2000. Seismic imaging of structural heterogeneity in earth's mantle: evidence for large-scale mantle flow, *Sci. Prog.,* **83,** 243–259.

Romanowicz, B., 2003. Global mantle tomography: progress status in the last 10 years, *Annu. Rev. Earth planet. Sci.,* **31**(1), 303–328.

Simmons, N.A., Forte, A.M. & Grand, S.P., 2007. Thermochemical structure and dynamics of the African superplume, *Geophys. Res. Lett.,* **34,** doi:10.1029/2006GL028009.

Simmons, N.A., Forte, A.M. & Grand, S.P., 2009. Joint seismic, geodynamic and mineral physical constraints on three-dimensional mantle heterogeneity: implications for the relative importance of thermal versus compositional heterogeneity, *Geophys. J. Int.,* **177,** 1284–1304.

Steinberger, B., 2000. Slabs in the lower mantle results of dynamic modelling compared with tomographic images and the geoid, *Phys. Earth planet. Inter.,* **118,** 241–257.

Steinberger, B. & Calderwood, A.R., 2006. Models of large-scale viscous flow in the earths mantle with constraints from mineral physics and surface observations, *Geophys. J. Int.,* **167,** 1461–1481.

Steinberger, B. & Holme, R., 2008. Mantle flow models with core-mantle boundary constraints and chemical heterogeneities in the lowermost mantle, *J. geophys. Res.,* **113,** doi:10.1029/2007JB005080.

Steinberger, B., Schmeling, H. & Marquart, G., 2001. Large-scale stress field and topography induced by global mantle circulation, *Earth planet. Sci. Lett.,* **186,** 75–91.

Steinberger, B., Sutherland, R. & O'connell, R.J., 2004. Prediction of Emperor-Hawaii seamount locations from a revised model of global plate motion and mantle flow, *Nature,* **430**(6996), 167–173.

Steiner, S.A. & Conrad, C.P., 2007. Does active upwelling help drive plate motion? *Phys. Earth planet. Inter.,* **161,** 103–114.

Torsvik, T.H., Steinberger, B., Gurnis, M. & Gaina, C., 2010. Plate tectonics and net lithosphere rotation over the past 150 my, *Earth planet. Sci. Lett.,* **291**(1–4), 106–112.

Wang, S. & Wang, R., 2001. Current plate velocities relative to hotspots: implications for hotspot motion, mantle viscosity and global reference frame, *Earth planet. Sci. Lett.,* **189,** 133–140.

Warners-Ruckstuhl, K.N., Meijer, P.T., Govers, R. & Wortel, M.J.R., 2010. A lithosphere-dynamics constraint on mantle flow: analysis of the Eurasian plate, *Geophys. Res. Lett.,* **37,** doi:10.1029/2010GL044431.

Wortel, M. J.R. & Vlaar, N.J., 1989. Subduction zone seismicity and the thermo-mechanical evolution of downgoing lithosphere, *Pure appl. Geophys.,* **128,** 625–659.

Wortel, M.J.R., Remkes, M.J.N., Govers, R., Cloetingh, S.A.P.L. & Meijer, P.T., 1991. Dynamics of the lithosphere and the intraplate stress field, *Phil. Trans. R. Soc. Lond. A,* **337,** 111–126.

Zhong, S., 2001. Role of ocean-continent contrast and continental keels on plate motion, net rotation of lithosphere, and the geoid, *J. geophys. Res.,* **106,** 703–712.

APPENDIX A: DYNAMIC MODELS OF LBFs

The net horizontal force F generated by topography variations is the horizontal derivative of the GPE P, which is derived from the integrated vertical stress of a lithospheric column (Artyushkov 1973; Fleitout & Froidevaux 1982; Molnar & Lyon-Cean 1988).

$$F_x = \frac{\delta}{\delta x} P, \quad F_y = \frac{\delta}{\delta y} P, \tag{A1}$$

$$P = \int_L^{-h} \left[\int_L^z \rho z' g \, \mathrm{d}z' \right] \mathrm{d}z, \tag{A2}$$

where z is depth ($z = 0$ at sea level), h is topography, L is the total depth, ρ is density and g is gravitational acceleration. In the case of isostatic equilibrium, L is the compensation depth at which pressure does not vary laterally. In our treatment of LBFs we allow for variations in dynamic support of the lithosphere by the mantle, expressed by pressure differences at depth L. Our results are sensitive to the choice of L, mainly in magnitude. To be consistent with mantle tractions obtained through mantle flow modelling assuming a constant lithospheric thickness of 100 km, the logical choice for L is 100 km.

We calculate the horizontal forces generated by topography variations using three end-member models for the lithospheric density distribution as a function of depth, on which we elaborate below. In contrast to the isostatically compensated models presented by Warners-Ruckstuhl *et al.* (2010), we treat the plate as one entity and include oceanic domains into the GPE calculations. In all models oceanic lithospheric thicknesses are deduced from the age of the lithosphere (Müller *et al.* 2008) and the boundary layer cooling model with constant basal heat flux, after Crough (1975), used in combination with parameter values derived by Wortel & Vlaar (1989).

A1 Model 'Mantle'

In model 'Mantle' we account for a dynamic contribution to topography generated by mantle convection. We use mantle flow modelling to calculated normal stresses on the base of the lithosphere (Milner *et al.* 2009).

In continental areas we assume that the part of the actual topography from ETOPO1 (Amante & Eakins 2009) that is not dynamically supported is isostatically compensated within the crust. The pressure difference between lithospheric columns at the base of the lithosphere is taken to equilibrate normal stresses due to mantle flow ($\tau_{\rm m}$). We work with constant crustal density $\rho_{\rm cr}$ and temperature-dependent lithospheric mantle density $\rho_{\rm m}(z)$, assuming a linear geotherm $T(z)$ throughout the lithosphere:

$$\rho_{\rm m}(z) = \rho_{\rm a}(1 + \alpha T(z)), \quad T(z) = T_{\rm a}\frac{z+h}{L+h}, \tag{A3}$$

$$\rho_{\rm av} = \frac{\rho_{\rm Moho} + \rho_{\rm a}}{2}, \quad \rho_{\rm Moho} = \rho_{\rm a}\left(1 + \alpha\left(\frac{T_{\rm a}h_{\rm cr}}{h+L}\right)\right), \tag{A4}$$

where $\rho_{\rm a}$ and $T_{\rm a}$ are the density and temperature of the asthenosphere, α is the thermal expansion coefficient, $\rho_{\rm av}$ is the average density of the lithospheric mantle and $\rho_{\rm Moho}$ is the density at sub-Moho depth.

Corresponding crustal thicknesses $h_{\rm cr}$ are calculated by comparison with a reference column of crustal and lithospheric mantle thicknesses $h_{\rm cref}$ and $h_{\rm mref}$ at sea level with zero normal mantle tractions. For regions above sea level:

$$h_{\rm cr} = h_{\rm cref} + h + \frac{h\rho_{\rm cr} + h_{\rm mref}\rho_{\rm avref} - \rho_{\rm av} - \tau_{\rm m}/g}{\rho_{\rm av} - \rho_{\rm cr}}. \tag{A5}$$

The GPE of a column above sea level then follows from eq. (A2):

$$P/g = \frac{1}{2}\rho_{\rm cr}h_{\rm cr}^2 + \frac{1}{2}\rho_{\rm Moho}(L+h-h_{\rm cr})^2 + \rho_{\rm cr}(L+h-h_{\rm cr})h_{\rm cr} - \frac{1}{6}\alpha\rho_{\rm a}\left(T_{\rm a} - \frac{T_{\rm a}h_{\rm cr}}{h+L}\right)(L+h-h_{\rm cr})^2. \tag{A6}$$

A similar equation can be formulated for continental regions below sea level, which we include for depths up to −1 km to exclude trenches where flexure is dominant and our assumptions are not appropriate.

In the oceans, lithospheric structure and reference bathymetry is deduced from secular cooling. We assume a constant 6 km crustal layer above the cooling lithosphere. The height of the lithospheric column is subsequently altered by adding the dynamic topography component caused by normal mantle tractions. This means that ocean depth in this model does not necessarily correlate with observed bathymetry. For theoretical bathymetry due to cooling of the lithosphere $h_{\rm theor}$, ocean depth becomes

$$h = h_{\rm theor} + \frac{\tau_{\rm m}}{g(\rho_{\rm a} - \rho_{\rm w})} \tag{A7}$$

yielding GPE of an oceanic column of

$$\begin{aligned} P/g = {} & \frac{1}{2}\rho_{\rm w}h^2 + \frac{1}{2}\rho_{\rm cr}h_{\rm cr}^2 + \frac{1}{2}\rho_{\rm a}(1+\alpha T_{\rm a})(h_L)^2 + \frac{1}{2}\rho_{\rm a}(L+h-(h_{\rm cr}+h_L))^2 - \rho_{\rm w}h(L+h) \\ & + \rho_{\rm cr}h_{\rm cr}(L+h-h_{\rm cr}) + \rho_{\rm av}h_L(L+h-(h_{\rm cr}+h_L)) - \frac{1}{6}\alpha\rho_{\rm a}T_{\rm a}(L+h-h_{\rm cr})^2. \end{aligned} \tag{A8}$$

Forces on the interface between continental and oceanic regions are govern by the choice of reference values for continental lithosphere and oceanic ridges and are excluded from the calculations.

A2 Model Crust2.0

Starting point for this model are seismological estimates of the lithospheric density structure. Topography, crustal thicknesses and densities are taken from model Crust2.0 (Bassin *et al.* 2000). The density of the lithospheric mantle linearly depends on temperature (eq. A3). Vertical stress integrals are calculated without assuming any kind of compensation. For areas above sea level GPEs follow from eq. (A6), continental regions below sea level yield GPE in a similar manner. Oceanic regions are treated in a way similar to continental regions, meaning actual bathymetry and crustal thicknesses are used. Lithospheric thicknesses are deduced from the theoretical secular cooling model used in model 'Mantle' and GPE follows from eq. (A8), replacing the conventional ridge push force.

Variations in pressure of the total lithospheric column at the base of the lithosphere illustrate deviations from local isostasy (Fig. A1). These variations should reflect normal stresses from the underlying mantle, although we note that lateral load variations on length scales up to 500 km can be supported by flexural strength of the lithosphere. Variations in supporting normal stresses at the base of model 'Crust2.0'

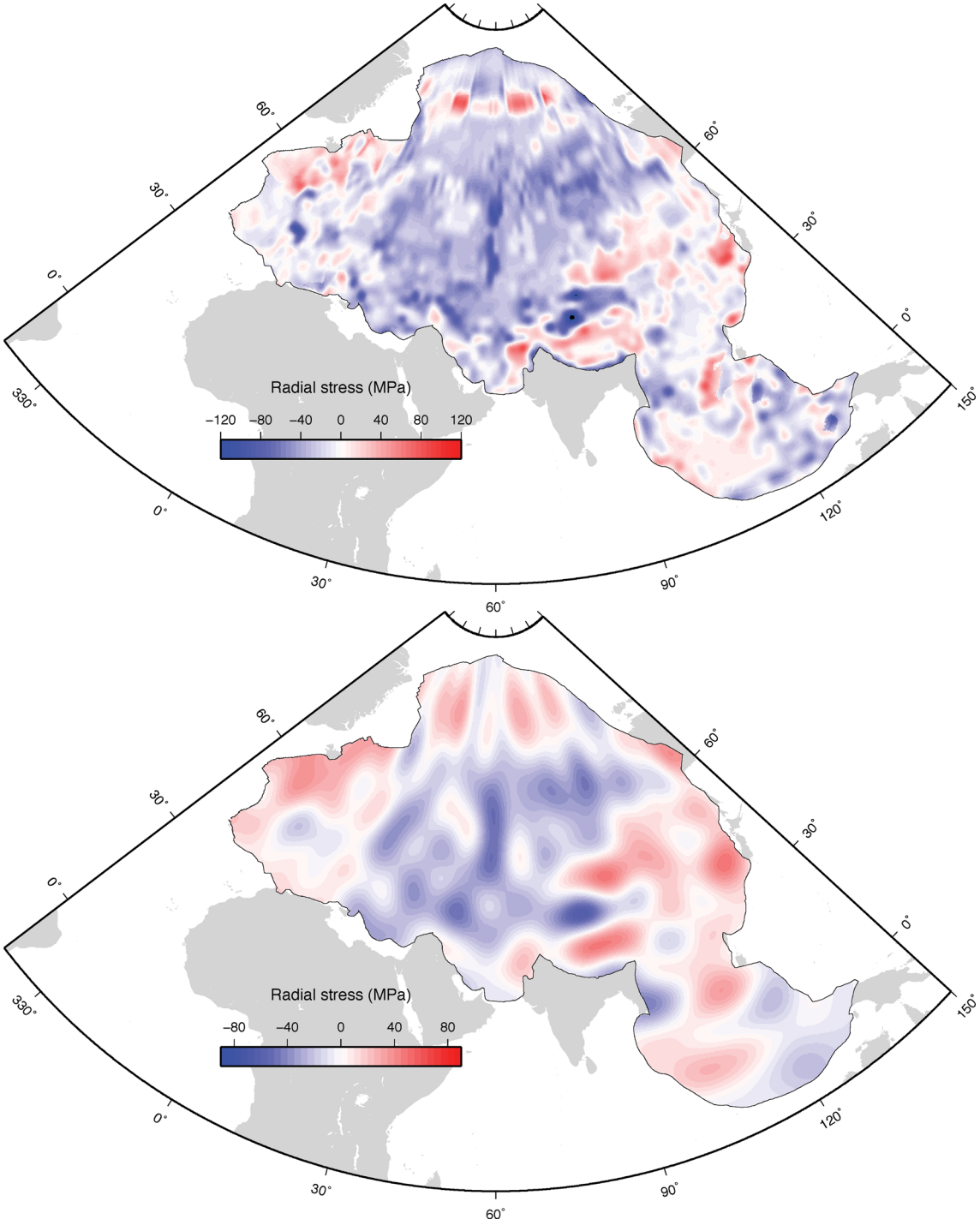

Figure A1. (a) Computed radial stress component at the base of the lithosphere that equilibrates model 'Crust2.0'. Upward stress is positive. (b) Same as (a), but filtered for the wavelength range of our mantle flow model results ($l_{max} = 31$). Compare with Fig. 3.

correlate with crustal thickness variations and occur on small length scale. To compare this field with normal stresses from mantle flow modelling (Fig. 3c, see main text), we apply a low-pass filter with the range corresponding to the mantle flow models ($l_{max} = 31$, wavelength larger than 1300 m).

A3 Model Lithodens

In this model, we combine crustal thickness and density from 'Crust2.0' with normal mantle tractions from mantle flow modelling. In essence, this model is similar to model 'Crust2.0'. However, averaged densities of the lithospheric mantle are adapted so that pressure overload from the lithospheric column matches variations in normal stresses from mantle flow modelling at its base. Lithospheric columns are compared to

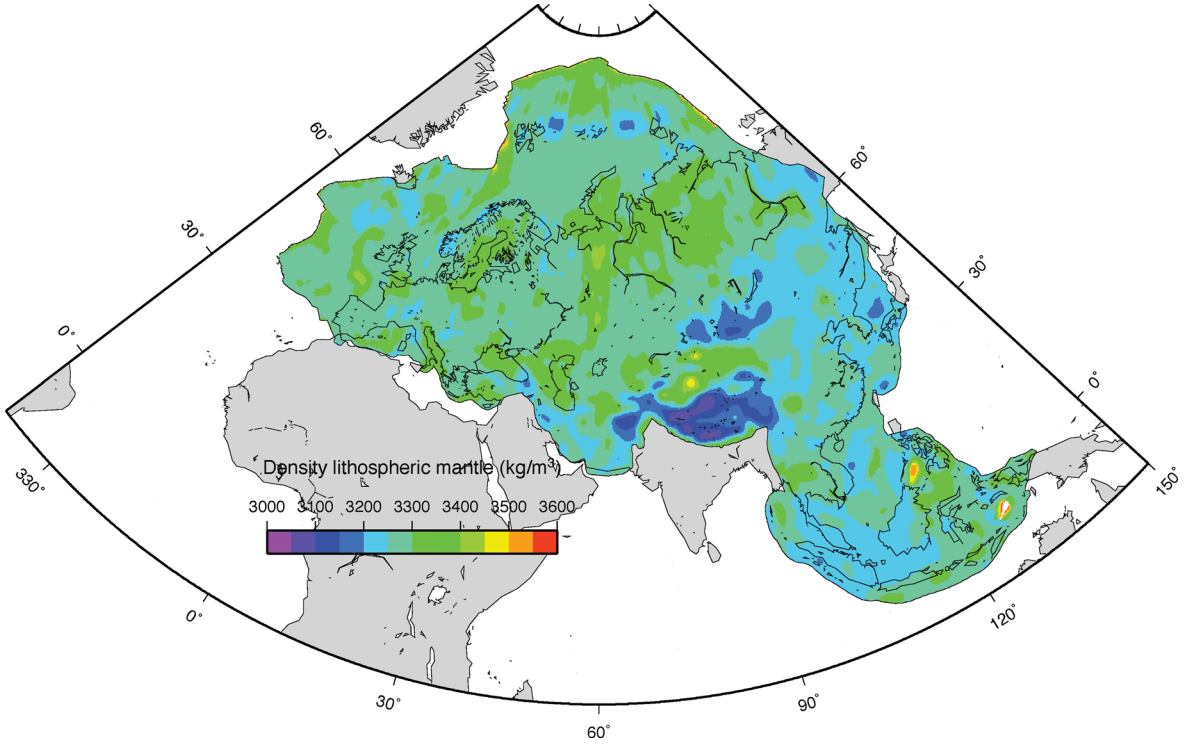

Figure A2. Computed lithospheric mantle densities that equilibrate model 'Lithodens'.

a reference lithospheric column at sea level with zero normal mantle tractions. For continents and continental margins we find ρ_m as follows:
Above sea level,

$$\rho_m = \frac{\rho_{cref} h_{cref} + \rho_{avref}(L - h_{cref}) + \tau_m/g - \rho_{cr} h_{cr}}{L + h - h_{cr}}. \tag{A9}$$

Below sea level,

$$\rho_m = \frac{\rho_{cref} h_{cref} + \rho_{avref}(L - h_{cref}) + \tau_m/g - \rho_{cr} h_{cr} + \rho_w h}{L + h - h_{cr}}. \tag{A10}$$

As we now have constant lithospheric densities, GPEs are given by the following:
Above sea level,

$$P/g = \frac{1}{2}\rho_{cr} h_{cr}^2 + \frac{1}{2}\rho_{Moho}(L + h - h_{cr})^2 + \rho_{cr}(L + h - h_{cr}) h_{cr}. \tag{A11}$$

Below sea level,

$$P/g = \frac{1}{2}\rho_{cr} h_{cr}^2 + \frac{1}{2}\rho_{Moho}(L + h - h_{cr})^2 + \rho_{cr}(L + h - h_{cr}) h_{cr} + \frac{1}{2}\rho_w h^2 - (L + h) h \rho_w. \tag{A12}$$

Oceanic regions are treated in a way similar to model 'Crust2.0'. However, as for the continental regions we now adapt lithospheric densities to match pressure at depth L with normal traction components from the mantle flow model.

$$\rho_m = \frac{\rho_{cref} h_{cref} + \rho_{avref}(L - h_{cref}) + \tau_m/g - \rho_{cr} h_{cr} + \rho_w h - (\rho_a(L + h - h_{cr} - h_L)}{h_L}. \tag{A13}$$

Table A1. Values used in LBF calculations.

Parameter	Symbol	Value
Crustal density	ρ_c	2850 kg m^{-3}
Crustal thickness reference column	h_{ref}	35 km
Asthenospheric density	ρ_a	3250 kg m^{-3}
Temperature asthenosphere	T_a	1200∘C
Thermal expansion coefficient	α	4×10^{-5}/∘C
Maximum depth of integration	L	100 km
Sea water density	ρ_w	1000 kg m^{-3}

Table A2. Abbreviation for model forces as used in figures.

ms	mantle shear
as	active shear
ps	passive shear
cd	LBF model 'Crust2.0'
md	LBF model 'Mantle'
ld	LBF model 'Lithodens'
cc af/ar/in/au	continental collision Africa/Arabia/India/Australia
cctot	total continental collision in case of equal forcing along entire continental boundary
ccin+ar	continental collision in case of equal forcing on Arabian and Indian boundary
tf	transform fault resistance
rb	force at trench roll-back margin
nrb	force at trench non-roll-back margins

GPE for oceanic regions is then

$$P/g = \frac{1}{2}\rho_{\mathrm{w}}h^2 + \frac{1}{2}\rho_{\mathrm{cr}}h_{\mathrm{cr}}^2 + \frac{1}{2}\rho_{\mathrm{m}}(h_L)^2 + \frac{1}{2}\rho_{\mathrm{a}}(L + h - (h_{\mathrm{cr}} + h_L))^2 - \rho_{\mathrm{w}}h(L + h) + \rho_{\mathrm{cr}}h_{\mathrm{cr}}(L + h - h_{\mathrm{cr}}) + \rho_{\mathrm{m}}h_L(L + h - (h_{\mathrm{cr}} + h_L)). \quad \text{(A14)}$$